Near-wall turbulence

Javier Jiménez

Additional information on Phys. Fluids

Near-wall turbulence

Javier Jiménez

School of Aeronautics, U. Politécnica de Madrid, 28040 Madrid, Spain

The current state of knowledge about the structure of wall-bounded turbulent flows is reviewed, with emphasis on the layers near the wall in which shear is dominant, and particularly on the logarithmic layer. It is shown that the shear interacts with scales whose size is larger than about one third of their distance to the wall, but that smaller ones, and in particular the vorticity, decouple from the shear and become roughly isotropic away from the wall. In the buffer and viscous layers, the dominant structures carrying turbulent energy are the streamwise velocity streaks, and the vortices organize both the dissipation and the momentum transfer. Farther from the wall, the velocity remains organized in streaks, although much larger ones than in the buffer layer, but the vortices lose their role regarding the Reynolds stresses. That function is taken over by wall-attached turbulent eddies with sizes and lifetimes proportional to their heights. Two kinds of eddies have been studied in some detail: vortex clusters, and ejections and sweeps. Both can be classified into a detached background, and a geometrically self-similar wall-attached family. The latter is responsible for most of the momentum transfer, and is organized into composite structures that can be used as models for the attached-eddy hierarchy hypothesized by Townsend ["Equilibrium layers and wall turbulence," J. Fluid Mech. **11**, 97–120 (1961)]. The detached component seems to be common to many turbulent flows, and is roughly isotropic. Using a variety of techniques, including direct tracking of the structures, it is shown that an important characteristic of wall-bounded turbulence is temporally intermittent bursting, which is present at all distances from the wall, and in other shear flows. Its properties and time scales are reviewed, and it is shown that bursting is an important part of the production of turbulent energy from the mean shear. It is also shown that a linearized model captures many of its characteristics. © *2013 AIP Publishing LLC*. [http://dx.doi.org/10.1063/1.4824988]

I. INTRODUCTION

A recurrent theme of turbulence research is the relationship between structure and statistics. Thus, while Richardson[2] framed the multiscale nature of turbulence in terms of "little and big whorls," the older decomposition of Reynolds[3] centered on the statistics of the fluctuations, and proved to be more fruitful for practical applications. Even the classical paper of Kolmogorov,[4] which is usually credited with introducing the concept of a turbulent cascade, is a statistical description of the fluctuation intensity versus scale, and it was only the slightly less famous companion paper by Obukhov[5] that put it in terms of interactions among eddies.

Up to the second part of the 20th century, the statistical approach was probably inevitable, because it is difficult to extract structural information from single-point measurements. It was not until the visualizations of large coherent structures in free-shear layers by Brown and Roshko,[6] and of sublayer streaks and ejections in boundary layers by Kline *et al.*,[7] and in pipes by Corino and Brodkey,[8] that the structural point of view began to gain modern acceptance. It was only after probe rakes, numerical simulations, and particle image velocimetry experiments started to routinely provide multidimensional flow fields that it became fully established. In the same way, the recent introduction of time-resolved three-dimensional flow information, currently almost exclusively from simulations,[9–11] promises a new impulse to structural turbulence dynamics.

The outlook of this paper is structural, treating turbulence as a property of deterministic solutions of the Navier–Stokes equations rather than as a stochastic process. As such, although it incorporates experimental data whenever available, it relies heavily on numerical results, not only because they usually provide more complete information than experiments, but for their ability to manipulate the equations of motion in ways that are not necessarily realizable in a laboratory.[12] Those conceptual methods have a long tradition in physics, where some of the most powerful tools have always relied on "thought" experiments involving "unphysical" concepts, for example, point masses. In simple dynamical situations, the outcome of such exercises can often be guessed and used to judge the soundness of a particular model, but in complex cases such as turbulence, the guessing almost always has to be substituted by the numerical simulation of the modified system.

The emphasis on structure does not reduce the importance of statistics. We said at the beginning that the statistical Reynolds[3] decomposition proved to be more practical in applications than earlier structural approaches, and it cannot be forgotten that turbulence is as important for engineering as it is for science. Moreover, statistics are required even when analyzing structure. Turbulent flows are chaotic and high-dimensional,[13, 14] and even if dissipation probably restricts them to a finite-dimensional attractor in phase space,[15] important aspects such as the inertial energy cascade are inviscid, and approximately conserve phase volume.[16, 17] Such systems explore their phase space uniformly and, in essence, anything that is not strictly inconsistent with the equations of motion is bound to occasionally happen. It is therefore important to approach structure identification statistically, and to make sure that any phenomenon that is observed, even if intellectually appealing, occurs often enough to be relevant to the overall dynamics of the flow. On the other hand, rare events can be important if they can be exploited for control purposes,[18] and turbulence, as a prime example of macroscopic chaos, may be one of the first systems in which we may hope for the engineering implementation of a "Maxwell demon," in the sense of extracting useful work from apparently random fluctuations.

In this paper, we are primarily interested in wall-bounded turbulent flows, particularly in those layers near the wall that are dominated by the shear. We will restrict ourselves to pipes, channels, and boundary layers with little or no longitudinal pressure gradients, since otherwise the flow tends to laminarize or to separate, and changes character. Wall-bounded flows are inhomogeneous and anisotropic and, even if turbulence was first studied scientifically in them,[19, 20] they remain in many ways worse understood than their homogeneous or free-shear counterparts.

On the other hand, some processes are easier to analyze in wall turbulence than in other apparently simpler cases. In the classical conceptual model for isotropic turbulence, energy resides in the largest eddies and is dissipated in smaller viscous scales of the order of the Kolmogorov length, to where it is transferred by a self-similar "inertial" cascade.[2, 4] The resulting energy spectrum closely approximates the experimental observations, not only for isotropic turbulence, but for small-scale turbulence in general. Unfortunately, isotropic theory gives no indication of how energy enters the turbulent cascade, and isotropic flows have no preferred spatial orientation to assist in organizing their study. In shear flows, the energy source is the gradient of the mean velocity, and energy enters turbulence through the interaction of that gradient with the transverse velocity fluctuations.[13] That generally provides a well-defined scale for the energy-containing eddies, as well as a spatial direction along which some properties are transferred, usually momentum. In addition, wall-bounded flows are inhomogeneous, and their eddy sizes are organized in terms of their distance to the wall. The result is that different eddies can be studied in relative isolation from one another. Moreover, momentum is injected away from the wall, usually by a pressure gradient, and removed at the wall by friction, while the scale stratification just mentioned requires that the structures have to change size as they transfer momentum between those two locations. Thus, wall-bounded turbulence provides an example of a multiscale "cascade" in which the locations of the sources and the sinks are known and spatially distinct. In that sense, and in spite of its apparent complication, it is probably a simpler system to analyze than other flows, and it may be our best current hope of fully describing a multiscale turbulent process.

Wall-bounded turbulence is also of huge technological importance. About 25% of the energy used by industry and commerce is spent in moving fluids along pipes and canals, or vehicles

through air or water,[21] and about one quarter of that energy is dissipated by turbulence in the immediate vicinity of walls. In terms of a quantity of current topical interest, shear-dominated wall-bounded turbulence is responsible for about 5% of the CO_2 dumped by mankind into the atmosphere.

We denote by x, y, and z the streamwise, wall-normal, and spanwise coordinates, respectively, and the corresponding velocity components by u, v, and w. Repeated indices imply summation from x to z. If we conceptually define the average $\langle\rangle$ over an ensemble of equivalent independent experiments, capitals are used for mean values, such as in $U = \langle u \rangle$, tildes denote fluctuations with respect to those means, $\tilde{u} = u - U$, and primes are root-mean-squared fluctuation intensities. We use δ for the 99% thickness of boundary layers, for the half-width of channels, and for the radius of pipes. "Wall" units are constructed with the kinematic viscosity ν and with the friction velocity $u_\tau = (\tau_w/\rho)^{1/2}$, defined in terms of the shear stress τ_w at the wall and of the fluid density ρ. Magnitudes expressed in those units are denoted by "+" superscripts. We will always assume that the fluid density is $\rho = 1$, and drop it from the equations. Our primary Reynolds number is δ^+, which measures the ratio between the length scales of the largest structures of the outer flow and those of the viscous eddies near the wall.

Recent reviews of particular aspects of wall-bounded turbulence related to the ones discussed here can be found in Refs. [22–27]. In our case, and given our intended use of numerical results, it may be useful to add a few words on the present status of simulations of wall-bounded turbulence. The first direct numerical simulations (DNS) of turbulent channels[28] appeared soon after computers became powerful enough to allow the simulation of turbulence in general,[29,30] although their Reynolds numbers, $\delta^+ \approx 180$, initially provided a very limited range of scales. However, Reynolds numbers steadily increased with the advent of more powerful computers, and recent numerical channels,[31–33] boundary layers,[34–40] and pipes,[41–43] with $\delta^+ \approx 1000 - 2000$, are comparable to most well-resolved experiments, and have a full decade of scale disparity. The next generation of simulations is beginning to appear. We use in this paper a numerical channel at $\delta^+ \approx 4200$, computed in a medium-sized box ($L_x = 2\pi\delta$, $L_z = \pi\delta$)[44] using the same code as in Ref. [33], which is useful for many particular purposes. A compressible boundary layer at roughly the same Reynolds number was recently published,[45] and simulations of pipes at $\delta^+ = 1800$ from the group at Delft, and at $\delta^+ = 3000$ from the one at KAIST in Seoul, have recently been presented at conferences. Two simulations of reasonably large channels in the range $\delta^+ \approx 4000 - 5000$, from the groups at the University of la Sapienza in Rome and at the University of Texas in Austin, are currently at different stages of execution. Most of these simulations will probably become available within the coming year.

It is important to realize that the process of increasing the Reynolds number need not be open-ended. The goal of turbulence theory, and of the supporting simulations and experiments, should not be to reach ever increasing Reynolds numbers, but to describe turbulence well enough to make useful predictions. It is probably true that, if we could compile a detailed database of the space-time evolution of enough flows with a reasonably wide range of scales, such a database would contain all the information required to formulate a theory of turbulence. Of course, such a data set would not be a theory, but it is doubtful whether further increasing the Reynolds number of the simulations, or of the experiments, would provide much additional help in formulating one.[24]

It is difficult to say *a priori* when that stage will be reached, since there may be Reynolds number effects about which we know nothing at present, but it is probably true that $\delta^+ = 10\,000 - 20\,000$, with a range of scales close to 100, would provide all the information required to understand most of the dynamical aspects of wall-bounded turbulence. Using the usual estimate of δ^{+3} for the cost of simulations, and the present rate of increase in computer speed of 10^3 per decade, it should be possible to compile such a database within the next decade.[46]

The organization of this paper is as follows. Section II reviews the classical theory of wall turbulence, defines the different regions of the flow, and summarizes how turbulence interacts with the mean shear. Section III reviews the kinematics of the structures and eddies of the shear-dominated layers, and Sec. IV studies their dynamics. Each of these last two sections is divided into subsections for the buffer and for the logarithmic layers. Section V concludes.

II. THE CLASSICAL THEORY

Wall-bounded turbulence over smooth walls can be described by two sets of scaling parameters.[13] In flows with a moderate pressure gradient, the friction velocity remains the characteristic velocity across the flow, because the momentum balance requires that the tangential Reynolds stress $-\langle uv \rangle$ remains approximately equal to $\tau_w = u_\tau^2$. As a consequence, $u' \propto v' \propto u_\tau$ unless the two velocity components decorrelate from one another.[13] The relevant outer length scale is the flow thickness δ, but the momentum-carrying structures near the wall are limited to sizes of the order of the viscous length scale, ν/u_τ, or of some other length connected, for example, with roughness. In both cases, the defining characteristic of attached wall-bounded turbulent flows is a uniform velocity scale, and distinct inner and outer lengths whose ratio plays the role of a Reynolds number. Here, we will center on the smooth-walled case in which the relevant Reynolds number is $\delta^+ = u_\tau \delta/\nu$. It varies from a few hundreds for barely turbulent flows, to 10^6 in big ships, in the atmosphere, or in large pipelines.

Figure 1(a) displays the premultiplied spectra of the wall-normal velocity and of the enstrophy, used as a surrogate for dissipation, as functions of the distance to the wall and of the spanwise wavelength, defined in terms of the wavenumber as $\lambda_z = 2\pi/k_z$. As usual, the velocities and the kinetic energy reside in long wavelengths, and dissipation in short ones, with an inertial range in which both are small, but where the inter-scale energy flux is expected to take place.[4] The result of the disparity of the inner and outer length scales is that the length of the inertial range changes with the distance to the wall, dividing the flow into distinct layers. Near the wall, the lengths and velocities scale in wall units, and Figure 1(a) shows that the energy and the dissipation are at similar sizes. Although we will see later that some large but flat eddies exist in this region, most large eddies are excluded by the impermeable wall, which inhibits wall-normal velocity. Because of the latter, there are no tangential Reynolds stresses in this layer, and the shear has to be strong for viscosity to carry all the tangential stress. This introduces a fast time scale, of the order of the viscous one, that prevents eddies from growing. If y is the distance to the wall, y^+ is a Reynolds number for the size of the structures, and it is never large within this viscous layer, implying that the eddies in this region are relatively smooth and can be described as simple structures.[25] This layer is typically defined at most as $y^+ \lesssim 150$,[48] although the precise limit depends on the application, and has been drawn in Figure 1(a) at $y^+ = 80$. It is conventionally divided into a viscous sublayer, $y^+ \lesssim 5$, where viscosity is dominant, and a "buffer" layer in which both viscosity and inertial effects should be taken into account.
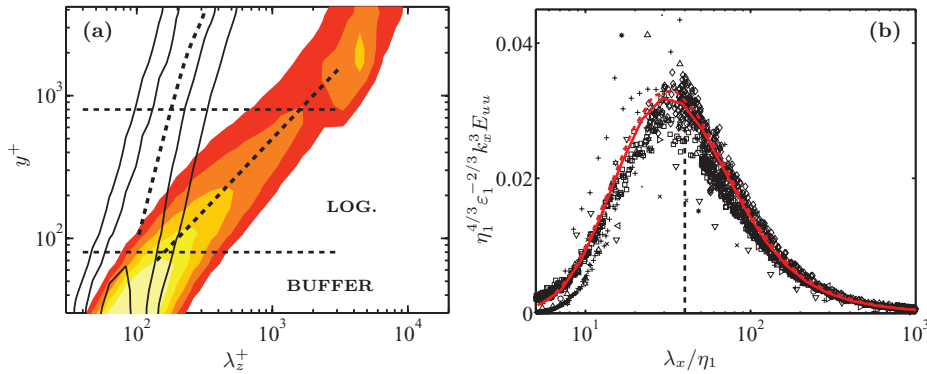

FIG. 1. (a) One-dimensional premultiplied spectra of the wall-normal velocity $k_z E_{vv}^{(1)}(k_z)$ (shaded) and of the surrogate energy dissipation $k_z E_{\omega\omega}^{(1)}(k_z)$ (contours), as functions of the spanwise wavelength, $\lambda_z = 2\pi/k_z$, and of the distance to the wall. Channel at $\delta^+ = 4200$.[44] The two dashed horizontal lines are $y^+ = 80$ and $y/\delta = 0.2$, representing conventional limits for the logarithmic layer. The dashed diagonal through the velocity spectrum is $\lambda_z = 2y$, and the one through the dissipation spectrum is $\lambda_z = 40\eta$. (b) Spectra of the longitudinal velocity gradients, in Kolmogorov scaling. The symbols are premultiplied spectra of $\partial_x u$ in a variety of experimental flows with $Re_\lambda = 50 - 3000$, extracted from Figure 9 in Ref. 47. The solid line is the spectrum of $\partial_x u$ in the same channel as in (a), at $y^+ = 1250$ ($Re_\lambda \approx 250$). The dashed line is $\partial_z w$. The vertical dashed line is 40η.

Farther away from the wall, where $y^+ \gg 1$ and $y \ll \delta$, neither the wall thickness nor the viscosity are relevant, and the only available length scale is the wall distance y.[49] How far this region extends into the flow depends on the variable being considered and on the type of flow. In the particular case of the wall-normal velocity in Figure 1(a), the wavelength of the spectral peak stays proportional to y across most of the flow, but a more conventional limit is $y/\delta = 0.15 - 0.2$.

Both the constant velocity scale across the intermediate region, and the absence of a length scale other than y, are only approximations but, if they are accepted as the first terms of a higher-order asymptotic expansion,[50–52] dimensional analysis implies that the mean shear has the form $S \equiv \partial_y U = u_\tau / \kappa y$, where the Kármán constant $\kappa \approx 0.4$ is approximately universal.[13,49] That equation can be integrated to give a logarithmic profile for the mean velocity,

$$U^+ = \kappa^{-1} \log y^+ + A, \tag{1}$$

which gives the overlap layer its name, and agrees reasonably well with experimental evidence.[48,53] Note, however, that the logarithmic layer is defined by the linear dependence of the length scale with y, rather than by (1).[13,49] Neither that linear dependence, nor the logarithmic profile, extend all the way to the wall, so that the intercept constant A acts as an inner boundary condition that depends on the details of the near-wall region. For smooth walls, $A \approx 5$.

The behavior of the small-scale end of the turbulent spectrum is closer to that of turbulence in general. Figure 1(a) shows that the vorticity resides near $\lambda_z \approx 40\eta$, where the Kolmogorov length is defined from the kinetic-energy dissipation ε as $\eta = (\nu^3/\varepsilon)^{1/4}$, and we have disregarded the effect of anisotropy because it will be seen below that the vorticity tends to become isotropic as y^+ increases. In the same way, we define an isotropic microscale Reynolds number $Re_\lambda = q^2 (5/3\nu\varepsilon)^{1/2}$, where $q^2 = u'_j u'_j$ is the magnitude of the velocity fluctuations.[54] If we assume that $q \approx u_\tau$, and that the dissipation is roughly equal to the energy production per unit mass, which in the logarithmic layer is $-\langle uv \rangle S \approx u_\tau^3/\kappa y$, the microscale Reynolds number is $O(y^{+1/2})$. A very rough approximation is $Re_\lambda = 7y^{+1/2}$, and the edge of the buffer layer, at $y^+ \approx 100$, corresponds to $Re_\lambda \approx 70$.

The length scale of the velocity gradients is tested in Figure 1(b) for a wide variety of flows with $Re_\lambda = 50 - 3000$. That figure uses spectra of the longitudinal velocity gradient, $\partial_x u$, which is available from experiments, and the normalization is done with the one-dimensional surrogate dissipation $\varepsilon_1 = 15\langle(\partial_x u)^2\rangle$, which is also the one used in experiments. In numerical channels, ε_1 underestimates the true dissipation by 10%–30% depending of y^+, but it has been kept for consistency. The wall distance chosen for the comparison, $y/\delta = 0.3$, is representative of the outer logarithmic layer, and corresponds to the maximum Re_λ. The agreement is excellent, suggesting that the small scales of wall turbulence are essentially similar to those of isotropic or free-shear flows.[47] Note that the figure includes the spectra of both $\partial_x u$ and $\partial_z w$ for the channel, and that they agree well, suggesting that the velocity gradients are very close to being isotropic in the wall-parallel directions.

A. The shear-dominated layers

Because the shear decays with the distance to the wall, the viscous, buffer, and logarithmic layers are the most characteristic features of wall-bounded flows, and account for a major part of the total energy production and dissipation, even if they are geometrically thin.

If we assume that the buffer layer extends to $y^+ \approx 100$, its fraction of the total thickness, $O(100/\delta^+)$, becomes negligible as the Reynolds number increases, while the logarithmic layer is always defined as about 20% of the boundary layer. On the other hand, we saw above that the energy production and dissipation above the buffer layer diverge towards the wall as u_τ^3/y, so that their integral up to a given height is $\int^y \varepsilon \, dy \sim u_\tau^3 \log(y^+)$. The result of this logarithmic behavior is that the fraction of the dissipation that takes place within the buffer layer decreases only logarithmically with the Reynolds number, while the one below the upper edge of the logarithmic layer increases logarithmically to unity as δ^+ increases. Once the empirical constants of those two logarithmic trends are adjusted to experiments, it turns out that, even at the highest realistic Reynolds numbers $\delta^+ = O(10^6)$, the total dissipation within the buffer layer is 25% of the total, while most of the rest takes place within the logarithmic layer. In the limit of infinite Reynolds number, all the dissipation would be in the logarithmic layer.
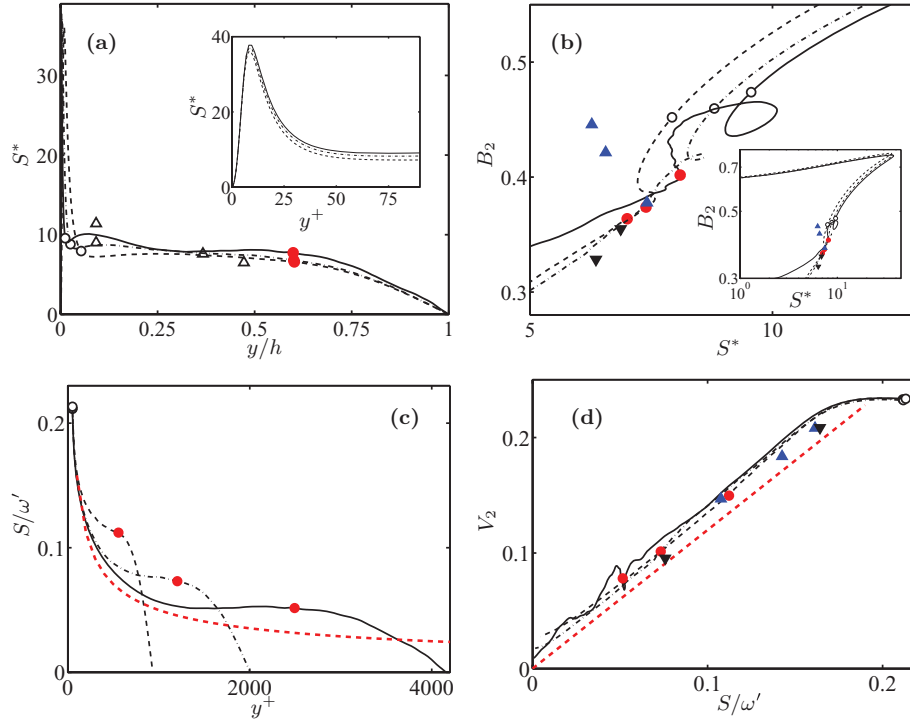
FIG. 2. (a) Shear parameter in wall-bounded turbulent flows, as a function of the distance to the wall. The inset is a detail in the buffer layer, in wall scaling. (b) Reynolds-stress anisotropy versus the shear parameter; see (2). The inset includes most of the channel below $y/\delta = 0.8$, while the larger plot is a magnification of the region including the logarithmic layer. (c) Shear-to-vorticity ratio, as a function of the wall distance. The thick dashed line is (3). (d) Vorticity anisotropy versus the shear-to-vorticity ratio; see (4). The thick dashed line is $V_2 = 1.2 S/\omega'$. Channels: – – –, $\delta^+ = 934$;[31] – · – · –, 2003;[33] ——, 4200.[44] △, High-Reynolds-number boundary layer;[47] $y^+ = 3 \times 10^3 - 6 \times 10^4$. Statistically steady homogeneous shear: ▲, $Re_\lambda = 50 - 90$;[55] ▼, $Re_\lambda = 50 - 120$.[56] The open and closed circles in all figures are, respectively, $y^+ = 50$ and $y/\delta = 0.6$, and are intended to represent limits for the region of constant S^*.

An interesting question is how similar is wall-bounded turbulence to other shear flows. A measure of the importance of the interaction of the shear with the energy-containing eddies is the parameter $S^* = Sq^2/\varepsilon$, which was introduced by Corrsin[57] to measure the ratio between the energy-decay time, q^2/ε, and the shear deformation time $1/S$. If $S^* \gg 1$, the mean shear dominates, and the evolution of the turbulent scales can be approximated as being controlled by the mean flow,[58] while $S^* \lesssim O(1)$ implies that turbulence can decouple from the shear, and nonlinearity prevails.

Figure 2(a) displays S^* as a function of the wall distance for boundary layers and channels. The flow can be divided into three parts. In the viscous layer below $y^+ \approx 50$, S^* reaches up to approximately 40, and the flow shares many of the characteristics of linearized rapid-distortion theory.[59] Above $y/\delta \approx 0.6$, S^* decreases towards zero, and shear is unlikely to play a major role. In between those limits, roughly coinciding with the extent of the logarithmic layer, $S^* \approx 10$ remains large and constant, and shear can be expected to be significant for the flow dynamics.[58]

A simple way to quantify the effect of the shear on a given range of scales is to measure their anisotropy. For the energy-containing eddies, a convenient measure is the second invariant $B_2 = (3b_{ij}b_{ij}/2)^{1/2}$ of the Reynolds-stress anisotropy tensor,[60]

$$b_{ij} = \frac{\langle u_i u_j \rangle}{|u|^2} - \frac{1}{3}\delta_{ij}, \qquad (2)$$

where the subindices range from x to z, and δ_{ij} is Kronecker's delta. The anisotropy B_2 ranges from unity for velocities which are perfectly aligned to some direction, to zero for completely isotropic ones,[60, 61] and is plotted against the shear parameter in Figure 2(b). Points in the buffer layer are in the upper-right part of the figure, and the distance to the wall increases towards the lower-left corner.

The logarithmic layer is represented by the central part, where $S^* \approx 7 - 10$. The different Reynolds numbers collapse well near the wall, corresponding to the upper branch in the inset, but they diverge as they move away from it, and the behavior in the logarithmic layer is only universal in the roughest sense. In particular, there is no clear tendency to a limit as δ^+ increases, and the anisotropy in the logarithmic layer actually appears to increase with the Reynolds number (for example, see the open circles at constant y^+). The figure includes some data from homogeneous shear. Homogeneous shear turbulence is not statistically steady,[62] but it reaches a statistically steady state when simulated in a finite box that limits the growth of the integral scale.[55,56] Some of those cases are included in Figure 2(b) and fall in the same region as the logarithmic layer, especially for the higher Reynolds numbers, but the agreement is again only approximate. Although not included in Figure 2(b) to avoid clutter, points from the centerline of plane shear layers cluster near the lower-right corner of the figure, underscoring the differences mentioned in the Introduction between shear flows whose mean velocity profiles are linearly stable or unstable.

The previous analysis only applies to the largest scales. Shear is important for structures of characteristic velocity u_ℓ and size ℓ if their time scale, $O(\ell/u_\ell)$, is slow compared to the mean shear S. If we assume the inertial relation,[4] $u_\ell \approx (\varepsilon\ell)^{1/3}$, that condition becomes $\ell > L_c = (\varepsilon/S^3)^{1/2}$, where the length L_c was introduced by Corrsin[57] as an upper limit for the isotropy of the small scales. It was later confirmed experimentally for boundary layers.[47] If we assume an equilibrium shear flow in which $\varepsilon \approx q^2 S$, the Corrsin length, $L_c = L_\varepsilon/S^{*3/2}$, becomes proportional to the integral energy scale $L_\varepsilon = q^3/\varepsilon$. In the logarithmic layer, $L_c \approx 0.3y$.

The smaller scales, and in particular the vorticity that resides in them, therefore tend to become independent of the shear above the buffer layer. If we assume that $\varepsilon \approx \nu\omega'^2$, it follows from the previous estimates that

$$S/\omega' \approx (\kappa y^+)^{-1/2}. \tag{3}$$

This approximation is tested in Figure 2(c), and works well in the logarithmic layer. It is known that vortices in a shear tend to orient along the most extensive strain direction at 45° to the stream,[62,63] but, if S becomes much smaller than ω', it is reasonable to expect that the vortices eventually decouple from the mean flow, and become roughly isotropic. For example, it is known that the magnitudes of the three vorticity components become approximately equal above $y^+ \approx 50$,[28] and we saw above that the spectra of the longitudinal velocity gradients also become isotropic in wall-parallel planes. A more complete measure of the isotropy of the orientation of the vorticity is the second invariant $V_2 = (3v_{ij}v_{ij}/2)^{1/2}$ of the anisotropy tensor,[55]

$$v_{ij} = \frac{\langle\omega_i\omega_j\rangle}{|\omega|^2} - \frac{1}{3}\delta_{ij}, \tag{4}$$

similar to the Reynolds-stress anisotropy used above. It can be expected that V_2 is proportional to S/ω' for weakly sheared flows,[64,65] and Figure 2(d) shows that this is true. The open and closed circles in Figure 2(d) mark the approximate lower and upper edges of the logarithmic layer, suggesting that the vortex alignment to the shear is essentially a low-Reynolds-number effect that disappears far from the wall. As δ^+ increases, the vorticity in the upper logarithmic layer becomes essentially isotropic, and is unlikely to play any role in interactions involving the shear, for example, momentum transfer. Note that the homogeneous shear flows,[55,56] included in Figures 2(b) and 2(d) agree with the channel data much better in the case of the vorticity than in the Reynolds stresses, in agreement with the intuitive idea that turbulence becomes more universal as the cascade progresses towards smaller scales.

In summary, the general picture from this section is that the buffer and logarithmic layers are shear-driven flows whose large scales interact strongly with the local shear, in a manner that can be only approximately modeled by the behavior of other shear flows. On the other hand, the small scales, including the vorticity, behave as in a slightly anisotropic homogeneous shear, and become increasingly uncoupled from the shear as the value of y^+ at the top of the logarithmic layer increases with increasing δ^+. In the rest of the paper, we will be mostly interested in the behavior of the larger scales, especially in the logarithmic layer, and in how they extract energy from the mean shear and
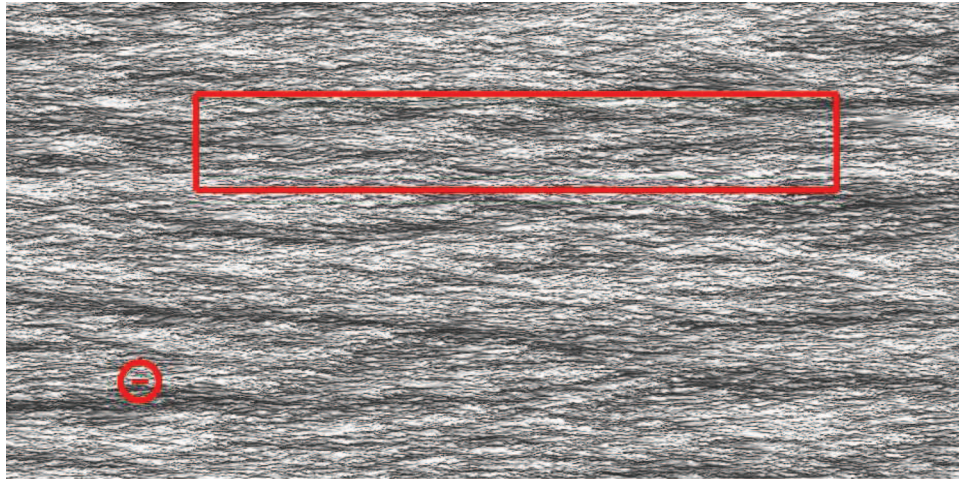
FIG. 3. Streamwise velocity in a wall-parallel plane in the buffer layer, $y^+ = 15$. Channel at $\delta^+ = 2003$.[33] The flow is from left to right, and the plane is approximately 3×10^4 by 1.5×10^4 wall units. Colors range from dark for $U^+ = 4.5$ to white for $U^+ = 17$. The small red rectangle (circled for clarity) is a minimal box of size 500×100 wall units. The larger rectangle is $10\delta \times 1.5\delta$.

transmit momentum across the variation of the integral length scale as a function of the distance to the wall.

III. STRUCTURES

A. The distribution of length scales

The spectra in Figure 1 do not represent the full complexity of the distribution of length scales, which depend on the variable involved. Consider first the buffer layer, whose streamwise velocity at the location of maximum fluctuation intensity is pictured in Figure 3. Its spectral energy density, $\phi_{uu} \equiv k_x k_z E_{uu}(k_x, k_z)$, is given at the bottom plane of Figure 4(a). It has two well-defined parts. The first one is the roughly elliptical region centered at $\lambda_x^+ \times \lambda_z^+ \approx 500 \times 100$, which is known to be very approximately independent of the Reynolds number.[33] It is dominated by coherent streaks of the streamwise velocity and by quasi-streamwise vortices. The former are an irregular array of long ($x^+ \approx 10^3$–10^4) sinuous alternating streamwise jets superimposed on the mean shear, with an average spanwise separation of the order of $z^+ \approx 100$.[66–68] They are the thinnest dark (low-velocity) lines in Figure 3. The quasi-streamwise vortices are slightly inclined away from the wall, and only stay in the buffer layer for lengths of the order of $x^+ \approx 100$, after which they merge into more disorganized vorticity away from the wall.[69] Several vortices are associated with each streak,[70] with a longitudinal spacing of the order of $x^+ \approx 300$. In Figure 3, they are represented by the white "speckle" of high-speed regions created by the downwash from individual vortices. Because vortices of different signs are, on average, staggered on opposite sides of the streaks,[71] they are responsible for the sinuous meandering that defines the streamwise wavelength of the maximum of ϕ_{uu}. In fact, it can be shown that the near-wall low-velocity streaks are wavy cylinders with a cross-section of aspect ratio roughly equal to one, and that even the longest ones are seldom wider[70] or taller[27] than 50 wall units. Meandering, as well as a certain amount of branching, is apparent in Figure 3, and has also been documented for the wider streaks of the logarithmic layer.[72]

The second important part of the spectrum is the diagonal "handle" in the far corner of the bottom spectral plane in Figure 4(a), which represents long and wide structures. This handle lies roughly along $\lambda_z = 0.15\lambda_x$, and gets longer as the Reynolds number increases.[33] The extra energy contained in it is responsible for the logarithmic growth with δ^+ of the streamwise velocity fluctuation intensity in the buffer layer.[33, 73–78] Although it is not clear whether there is an upper bound for the length of this large-scale spectral handle, other than the length of the simulation box or of the experimental
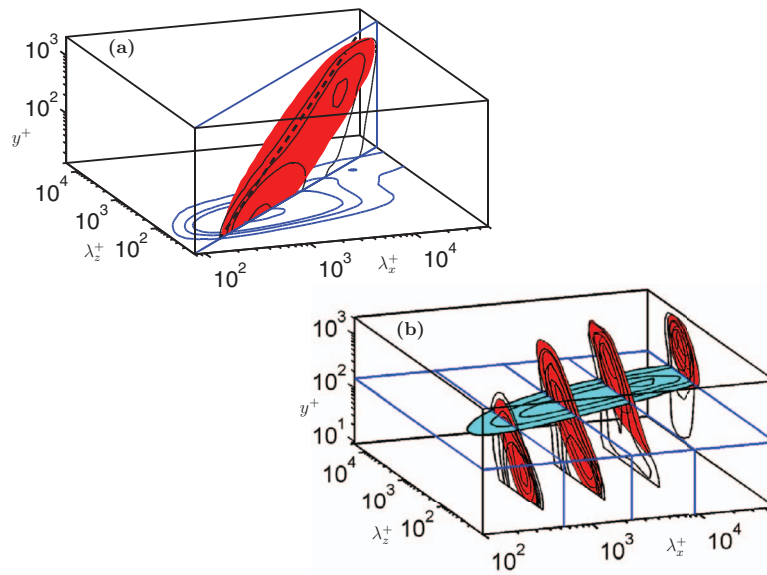
FIG. 4. Channel at $\delta^+ = 2003$.[33] (a) The bottom plane is $y^+ = 15$, and the diagonal wall-normal one is $\lambda_z = 0.15\lambda_x$. The contours in both planes are the two-dimensional spectral energy density $\phi_{uu} = k_x k_z E_{uu}(k_x, k_z)$ of the streamwise velocity, in terms of the streamwise and spanwise wavelengths, and of y. The contours are (0.1, 0.2, 0.3, 0.8) times the maximum of the spectrum at $y^+ = 15$. The shaded area in the diagonal plane is the premultiplied cospectrum of the tangential Reynolds stresses, $\phi_{uv} = -k_x k_z E_{uv} > 0.1$, normalized with its maximum. The dashed diagonal is $\lambda_z = 2y$, as in Figure 1(a). (b) The wall-parallel shaded contours are $\phi_{uu} = 0.3(0.2)0.9$ at $y/\delta = 0.075$ ($y^+ = 150$), normalized with its maximum. The wall-normal planes are $\lambda_x/\delta = (0.28, 1.2, 4.6, 25)$. The line contours in those planes are ϕ_{uu}, normalized as in the wall-parallel plane. The shaded ones are the same isocontours for the cospectra, normalized with their individual maxima.

record,[79] a representative limit for the available data in channels is $\lambda_x \times \lambda_z = 10\delta \times 1.5\delta$.[33] A rectangle with those dimensions has been added to Figure 3, where the large-scale modulation of the flow can be easily seen. Note the difference between these large-scale features and the dimensions of the individual streak/vortex units, whose characteristic size, $\lambda_x^+ \times \lambda_z^+ = 500 \times 100$, has also been added as a rectangle to Figure 3, highlighted by a circle to improve visibility. The large scales of boundary layers are shorter and narrower than in channels ($4\delta \times \delta$),[36,80,81] and the available data appear to be sufficient to rule out infinitely long structures in that case.

Mathis, Hutchins, and Marusic[82] noted that the coupling of the large-scale modulation with the near-wall structures is stronger than a simple linear superposition of the different spectral modes, and proposed a model in which the large scales act as a multiplicative factor for the small ones. It turns out that most of this coupling can be absorbed into the variability of the local friction velocity, which is modulated from place to place by the overlying large scales.[24] That makes sense, because Figure 3 shows that the sizes of the two kinds of structures are different enough for the elementary structures of the viscous layer to spend most of their "lives" in an environment defined by a single large-scale modulation. In fact, models with a variable friction velocity depending on the larger scales of the logarithmic layer have long been used as wall boundary conditions for large-eddy simulations, with relative success.[83–85]

That the large-scale modulation is associated with outer structures is shown by the diagonal wall-normal plane in Figure 4(a), which is a section through the premultiplied spectrum considered as a function of the two wall-parallel wavelengths and y. The spectrum of u is restricted to a roughly triangular "wedge" below $\lambda_x \approx 5y$, containing long and tall structures, at least some of which extend from their maximum height down to the wall. Those are the structures denoted by Townsend[1] as "attached." His argument was that, since turbulent energy resides in the largest scales of the spectrum, and the only obvious limiting mechanism for the size of those structures is the presence of the wall, the largest eddies would grow until becoming attached. Townsend[1] also noted that not all the flow variables can have attached structures, since the impermeability condition and

the resulting pressure effects prevent the wall-normal velocity of the large-scales from extending all the way to the wall. This is shown in the diagonal plane in Figure 4(a), where the cospectrum of the tangential Reynolds stresses is the shaded region restricted to a diagonal band away from the wall, approximately coinciding with the $\phi_{vv}^{(1)}$ spectrum in Figure 1(a). In general, the wall-parallel velocities and the pressure are attached, while the wall-normal velocity and the tangential Reynolds stress are detached.

A clearer representation of the structure of the spectra far from the wall is Figure 4(b), which centers on a wall-parallel section of ϕ_{uu} along a plane in the logarithmic layer. A dimensional argument similar to the one for the logarithmic mean velocity profile shows that neither y nor δ can be used to scale the energy spectrum for wavelengths that are much larger than y and much smaller than δ. If there is energy at those scales, the only possibility is that ϕ_{uu} and its one-dimensional analog $\phi_{uu}^{(1)} = k_x E_{uu}^{(1)}(k_x)$ are independent of the wavelength, and proportional to u_τ^2. Equivalently, the one-dimensional spectrum should be $E_{uu}^{(1)} \sim u_\tau^2 k_x^{-1}$.[86, 87] This is confirmed by the plateau in the horizontal section of ϕ_{uu} in Figure 4(b). The axis of that plateau, $\lambda_z \sim (y\lambda_x)^{1/2}$, can be interpreted as a self-similar conical structure of the velocity statistics,[31] agreeing with older theoretical models.[1, 88]

Note that only attached variables have k_x^{-1} spectra, because detached ones have no energy in wavelengths satisfying the above criteria. The vertical structure of the spectrum is represented in the several cross sections along the length of Figure 4(b), which show that ϕ_{uu} is indeed roughly independent of y near the wall, but that the cospectrum is detached, and stays bounded away from the wall, both for wide scales at any length, and for all the scales that are long and wide enough.

The structure just discussed for the spectrum implies that the near-wall roots of the large structures of u do not contain tangential Reynolds stresses, which is why they were described by Townsend[88] as "inactive." An interesting consequence is that, since the argument given above for the scaling of the velocity fluctuations with the friction velocity rests on the magnitude of the tangential Reynolds stress, the only part of the structures whose velocity is thus constrained is the active core at $y \sim |\lambda|$. The velocity scaling of the inactive roots can only be determined by their active cores, from where it is transmitted by the magnitude of the pressure fluctuations.[89] Indeed, in a numerical experiment in which the friction velocity was made to vary with height by the introduction of artificial volume forces,[90] the spectrum in the inactive wedge was found to scale with the friction velocity at the wall distance corresponding to the active structures with the particular wavelengths involved, rather than by the friction velocity at the wall.

Another consequence of the spectral structure just described is that the fluctuation profiles of the attached flow variables depend logarithmically on the distance to wall.[1, 88] This has often been discussed in terms of particular models for the flow structure, usually a forest of vortex hairpins,[68, 87, 91] but it is a more general property that follows directly from integrating the spectrum over the attached wedge discussed above as a dimensional necessity. For example, consider the premultiplied spectrum of u represented by the horizontal cross section in Figure 4(b). It can be approximated by a one-dimensional plateau of magnitude proportional to u_τ^2, extending from $\lambda_x \approx 10y$ to $\lambda_x \approx 25\delta$. The velocity intensity follows by integration

$$u'^2 = \int E_{uu}^{(1)} \, dk_x = \int \phi_{uu}^{(1)} \, d\log \lambda_x \propto u_\tau^2 \log(\delta/y). \tag{5}$$

This conclusion could not be confirmed experimentally for the streamwise velocity until recently,[68, 92, 93] probably because the strong signal from the streaks of the buffer layer requires very high Reynolds numbers before the logarithmic trend emerges. On the other hand, the logarithmic fluctuation profiles of the spanwise velocity and of the pressure are clear at more moderate Reynolds numbers, and were actually first documented in simulations.[36, 79, 94] The example of channels is given in Figure 5(a). The maximum of each quantity is reached at some fixed y^+, approximately independent of the Reynolds number, implying that the maximum intensity increases logarithmically with δ^+,[79] but the argument rests on the integration in (5), which includes the flow-dependent longest and tallest scales. The result is that the maximum value near the wall also depends on the type of flow.
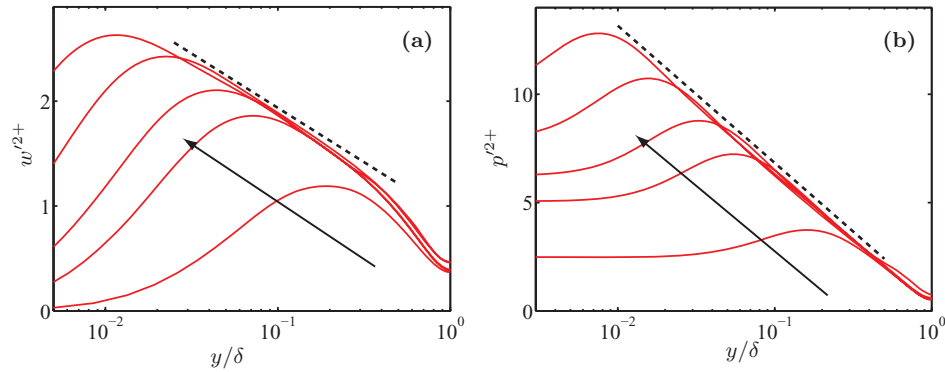
FIG. 5. Logarithmic profile of the fluctuation intensities in numerical channels, $\delta^+ = 180 - 4200$, increasing in the direction of the arrows. (a) Spanwise velocity. The dashed line is $w'^{2+} = 0.9 - 0.45 \log(y/\delta)$. (b) Pressure. The dashed line is $p'^{2+} = 0.5 - 2.75 \log(y/\delta)$.

That is particularly noticeable for the pressure fluctuations at the wall, as shown in Refs. [36] and [94], although Figure 5 only includes channels to avoid clutter.

B. The structures of the logarithmic layer

The structure of the flow becomes more complicated above the buffer layer, mainly because of the coexistence of multiple scales. We saw in Figure 1 that the scales of the vorticity and of the velocity diverge above $y^+ = 100$, and in Figure 3 that the difference between the scales of different parts of the flow can be considerable. Figure 6, which shows mostly structures reaching to the center of the channel, displays graphically the different organization of the velocity and of the vorticity. The streamwise velocity is organized into streamwise streaks, as in the buffer layer, but they are
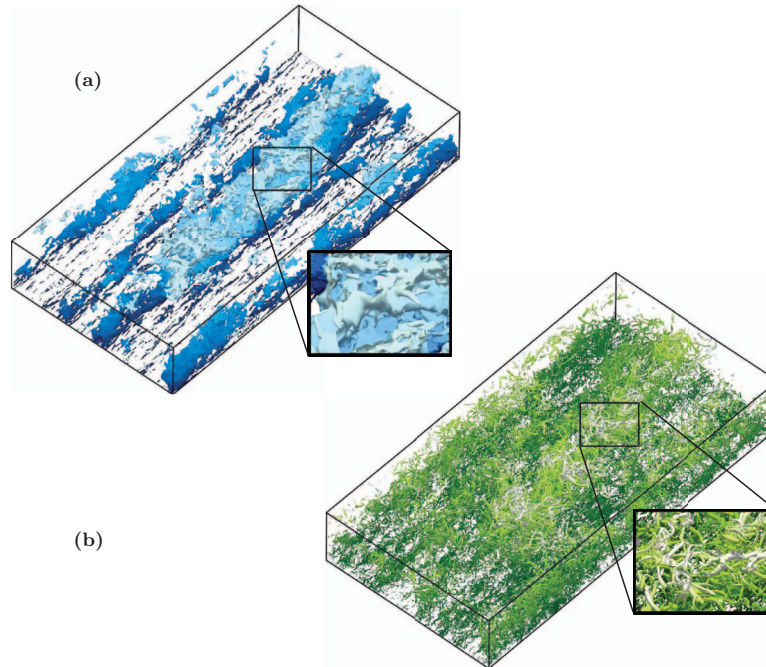

FIG. 6. Instantaneous snapshots of (a) low streamwise velocity; $\widetilde{u} < -1.5u'$. (b) Discriminant of the velocity gradient; $D > 0.02D'$.[95] Numerical channel at $\delta^+ = 2000$.[44] Flow is from bottom-left to top right, and the box is $2\pi\delta \times \delta \times \pi\delta$, approximately $12000 \times 2000 \times 6000$ wall units.

now much larger. The width of the single large low-velocity streak in Figure 6(a) is $z^+ \approx 3000$ ($z/\delta \approx 1.5$) rather than $z^+ = 50$, and it crosses the whole length of the simulation box. On the other hand, the organization of the vortices in Figure 6(b) is very different from those in the buffer layer (see, for example, any of the lower panels in Figure 10(b)). We saw in Sec. II A that vorticity tends to become more isotropic far from the wall, and Figure 6(b) confirms that it is difficult to discern any particular orientation or geometry of the individual vortices. As a consequence, the role of the vortices changes as we move away from the wall. As is true of all gradients, vorticity resides in the short end of the spectrum,[4] and shares the scales of the dissipation. In the buffer layer, because the vortices are mostly oriented streamwise, the up- and down-wash from individual vortices is also responsible for the tangential Reynolds stress. Above the buffer layer, the role of organizing the Reynolds stresses has to be taken over by other structures with sizes proportional to y rather than to η (see Figure 4(a)). We will refer to those larger structures as eddies.

The concept of eddy is linked to the structural rather than to the statistical approach to fluid mechanics. The general idea is that scales are localized in Fourier space, while eddies are localized in physical space. Tennekes and Lumley[13] proposed a kinematic definition of an eddy as an object with some localization in both spaces, somewhat similar to what we would now call an intense wavelet.[96,97] That point of view is similar to the one used by Obukhov[5] for his cascade scenario, where eddies are little more than Lagrangian fluid blobs, expected to remain coherent over turnover times defined from their dimensions and from their internal velocity differences. Later use of the word tended to refer to structures with longer coherence times, such as the kinetic-energy structures of free-shear flows,[6,98] or the intense vorticity structures of small-scale turbulence.[99–101] We will use the term here with the slightly different meaning of a spatially localized structure carrying some particularly interesting fluid property.

Two kinds of eddies have been studied in some detail for the logarithmic layer. The first ones are large-scale vorticity structures. The vorticity spectrum is localized at small scales, and it has been shown for a variety of flows that individual vortices have diameters of the order of a few Kolmogorov units.[101,104–107] However, vortices are not uniformly distributed,[101] and they cluster more strongly than what would be expected from purely Poisson statistics.[108] Vortex clusters in wall-bounded flows exist for all sizes, from the Kolmogorov to the integral scale,[95,103,109] and the larger ones are disorganized objects with no clear internal structure. They have fractal dimensions of the order of $D_F = 2$, which are different from those of the individual line-like vortices,[99–101] whose fractal dimension is $D_F \approx 1$.[108] This suggests that, statistically, they are shell-like aggregations of individual vortices, in agreement with qualitative visual observations.[101] An example of a cluster of roughly integral scale is Figure 7(a).

The second kind of eddies that have been studied in wall turbulence are Reynolds-stress structures (or "Q"s, for quadrant), which are three-dimensional analogs of the classical quadrant analysis
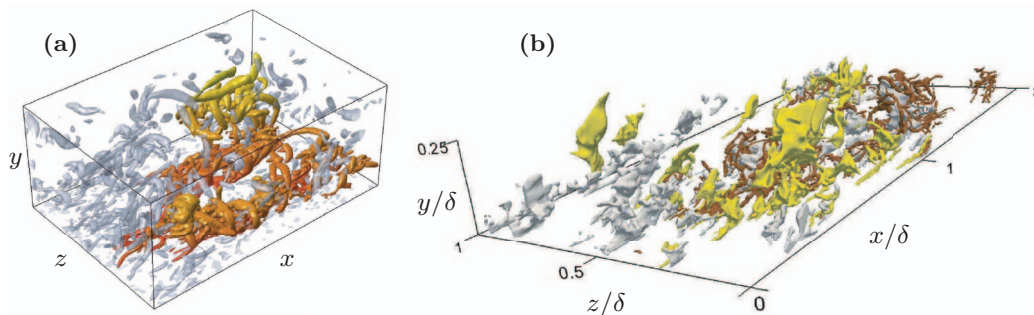

FIG. 7. (a) The solid object is a connected vortex cluster in a channel at $\delta^+ = 550$,[102] defined by a variable threshold of the discriminant of the velocity gradient.[95] Translucent objects are other vortices not in the cluster. The box is $2.7\delta \times 1.8\delta \times 0.9\delta$, or approximately $1500 \times 1000 \times 500$ wall units. (b) The lighter large objects are sweeps (yellow, darker) and ejections (gray, lighter), defined by $-uv > Hu'v'$, with $H = 1.75$.[103] The dark worm-like objects are vortex clusters as in (a). All objects are attached to the wall, and have maximum heights between $y^+ = 100$ and $y/\delta = 0.2$. Channel at $\delta^+ = 2003$. The flow is from left to right in (a) and (b).
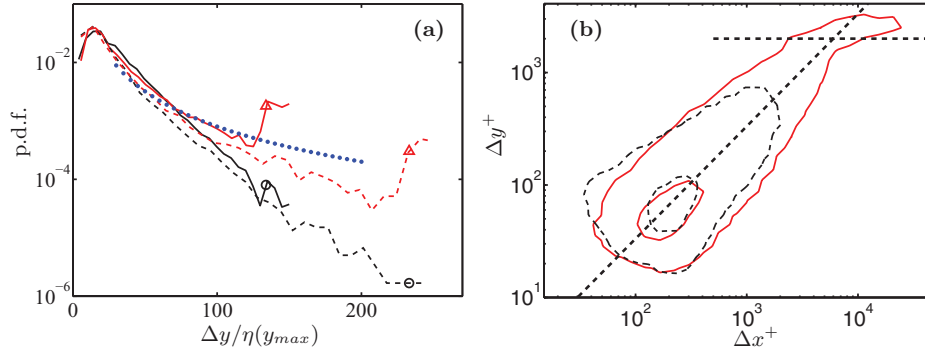
FIG. 8. (a) Probability density function of the vertical dimension, $\Delta y = y_{max} - y_{min}$, of: ○, vortex clusters, and △, ejections and sweeps (Q2 and Q4, $H = 1.75$). ——, $y_{max}/\delta = 0.3 \pm 0.02$; – – –, $y_{max}/\delta = 0.7 \pm 0.03$. Symbols mark $y_{min} = 0$. The dotted line is proportional to y^{-2}. (b) Joint p.d.f. of the logarithms of the sizes of the parallelepiped circumscribing attached ejections (solid lines), and vortex clusters (dashed). The contours contain 50% and 98% of the p.d.f. The dashed diagonal is $\Delta x = 3\Delta y$, the dashed horizontal line is $\Delta y = \delta$, and the top of the plot is the full channel height. Figure 8(b) is adapted from Ref. 103. Both figures are for a numerical channel at $\delta^+ = 2003$.[33]

of the shear stress.[110–113] Every point in the flow is classified in terms of its location in the parameter plane of streamwise and wall-normal velocity fluctuations. Objects with $\widetilde{v} > 0$, $\widetilde{u} < 0$ when $S > 0$ are ejections (second-quadrant, Q2) and those with $\widetilde{v} < 0$, $\widetilde{u} > 0$ are sweeps (Q4). Both quadrants transport streamwise momentum in the direction of increasing mean velocity, because $\tau = -\widetilde{u}\widetilde{v} > 0$. Points in the other two quadrants (Q1 and Q3, $\tau < 0$) transport momentum against the shear, but it is known that the pro-shear quadrants predominate.[110] Connected objects with $\tau > Hu'v'$ are defined as eddies responsible for strong momentum transfer. Earlier experimental experience with one-dimensional signals suggests using $H \approx 1.75$,[114] which approximately agrees with the percolation threshold of the three-dimensional objects.[103] An example of a group of large sweeps and ejections is Figure 7(b), which also includes vortex clusters in the same range of sizes. Sweeps and ejections have slightly fuller shapes than vortex clusters, with $D_F \approx 2.25$. They have been described as sponges of flakes, while the vortex clusters are sponges of strings.[103]

Both vortex clusters and Q's can be classified into families of wall-attached and wall-detached structures, where the former are defined as objects whose lowest point is $y_{min}^+ < 20$.[95,103] Most structures of both kinds are detached, as seen in Figure 8(a), which shows probability density functions (p.d.f.'s) of the vertical dimensions of structures whose tops, y_{max}, are in two narrow bands of wall distance. All the p.d.f.'s peak at size $\Delta y = y_{max} - y_{min} \approx 15\eta$, where the Kolmogorov scale is measured at y_{max}. That is approximately the diameter of individual small-scale vortices.[101] In this representation, it is difficult to see the signature of attached vortex clusters, but the attached Q's are clearly revealed by the sharp rise of their p.d.f.'s at $\Delta y \approx y_{max}$ ($y_{min} \approx 0$). Even if the attached eddies are relatively few, they are large enough to be important. For intense tall objects with $H = 1.75$ and $y_{max}^+ > 100$, the attached Q2's and Q4's represent 15% of the total number of sweeps and ejections, but they account for 82% of the total volume occupied by the Q2's and Q4's, and for 60% of the total tangential Reynolds stress. Attached clusters are less dominant: their equivalent percentages are 3% and 8%. It was shown by Lozano-Durán, Flores, and Jiménez[103] that detached Q's carry relatively little net Reynolds stresses because the detached Q1's and Q3's cancel the contributions of the detached Q2's and Q4's. In fact, detached Q's seem to be a feature of all turbulent flows, and their size distribution agrees well with the Reynolds-stress fluctuations in free-shear flows at high Reynolds numbers, including the centerline of jets in which the shear and the net tangential Reynolds stress vanish.[103] A typical size distribution for those statistically isotropic Reynolds-stress fluctuations is included as a dotted line in Figure 8(a), for comparison. Only when the roots of those eddies approach the wall is their statistical isotropy broken, most probably by the strong shear.

Attached Q's and clusters form geometrically self-similar families, with lengths and widths proportional to their heights, $\Delta x \approx 3\Delta y$ and $\Delta z \approx \Delta y$ (see Figure 8(b)). The largest ejections extend from the buffer layer to the opposite wall of the channel. Sweeps are somewhat lower than

ejections, but their number decays at a similar rate with the distance to the wall, and they also exist for all heights. On the other hand, the number of attached clusters decays faster than the Q's, and they essentially disappear for $y^+ > 800$ at all the Reynolds numbers investigated.[103] Note that Figure 8(b) does not represent the position of the eddies with respect to the wall, but their size, and that all the objects in the figure are attached. The figure is the equivalent of the spectra of Figure 4, and confirms that the attached spectra are due, at least in part, to individual attached structures.

The existence of attached sweeps, ejections, and vortex clusters appears to contradict the detached nature of the Reynolds-stress and vorticity spectra, but that is not the case. The cospectrum describes the structure of the Reynolds stress at a given height, but does not tell whether two objects that appear separated near the wall are parts of a connected single object further up. The conceptual model for a large attached ejection or sweep is a detached core with a self-similar fractal forest of "legs" reaching down to the wall. This can be checked directly by examining wall parallel sections of attached three-dimensional objects.

Sweeps, ejections, and clusters are not randomly distributed across the flow. It was shown by Lozano-Durán, Flores, and Jiménez[103] that, if the flow is conditioned to the position of a Q2, the most probable location of the next closest Q2 is either immediately ahead or behind it, in the streamwise direction. The same is true for the Q4's and for the clusters, all of which are aligned streamwise. On the other hand, Q2's and Q4's are located side by side in the spanwise direction, forming pairs. On average, the clusters are located between the two Q's, but closer to the ejection. Because of the right-left symmetry of the flow, the p.d.f. of the relative positions of two different kinds of structures is always statistically symmetric in the spanwise direction, independently of the symmetry of the individual groups of eddies. The latter can be tested by looking at the probability distribution of the location of the second-closest Q4 after orienting the frame of reference of each individual Q-pair so that the closest Q4 is always to the left of the Q2. If the individual groups were symmetric triples, as in a hairpin, the result would be a strong secondary probability peak in the side opposite to the primary one. What is found is that the secondary peak is weak or nonexistent, showing that the predominant structure is a single large-scale streamwise roller, rather than a more symmetric hairpin.[103]

The average structure of the composite object is shown in Figure 9(a), which displays isosurfaces of the p.d.f.'s of finding points belonging to the three kinds of objects. It is a self-similar statistical construct compiled from objects of different sizes in the logarithmic region ($y_{max}^+ > 100$), in the spirit of the VITA[115] and VISA[116] techniques in which bursts are rescaled according to their sizes. Before being added to the p.d.f., the coordinates of each object are centered at the center of gravity of the Q-pair, and scaled with the distance of that point to the wall, in such a way that the center of gravity of the pair is always at $y = 0$, and the wall is at $y = -1$. The pairs are then reoriented spanwise to a common polarity, as explained above. Figure 9(b) shows that, when a conditional velocity field is computed around these Q-cluster groups, they are found to sit at the boundary between a high- and a low-speed streak, with the ejection on the low-speed side, and the sweep on the high-speed one. Figure 9(c) represents the conditional vorticity, defined as the curl of the conditional velocity in Figure 9(b). In agreement with the discussion in the previous paragraph, it shows a single strong roller sitting between the sweep and the ejection, roughly coinciding with the mean location of the vortex cluster. The counterrotating vortices that flank it are much weaker and disorganized. The intensity of the main conditional roller, $O(u_\tau/y_{cg})$, is of the same order as the mean shear at the center of gravity of the eddy, $u_\tau/\kappa y_{cg}$, although, as we saw in Figure 2, it is much weaker than the characteristic vorticity of the individual vortices that form the cluster.

The location of the conditional roller in Figure 9(c), as well as the previously mentioned observation that the attached vortex clusters tend to be found only close to the wall, suggests that they are formed by random vortex debris advected by the ejection from the buffer layer into the outer flow, where they eventually dissipate.[95, 103] On the other hand, Figure 9(c) also shows that the vorticity in the cluster retains enough organization to induce a large-scale circulation that appears to be responsible for the sweep-ejection pair. Since velocity and vorticity are kinematically related, the two observations are not incompatible, and reinforce the conclusion that the three objects are parts of a single composite structure.
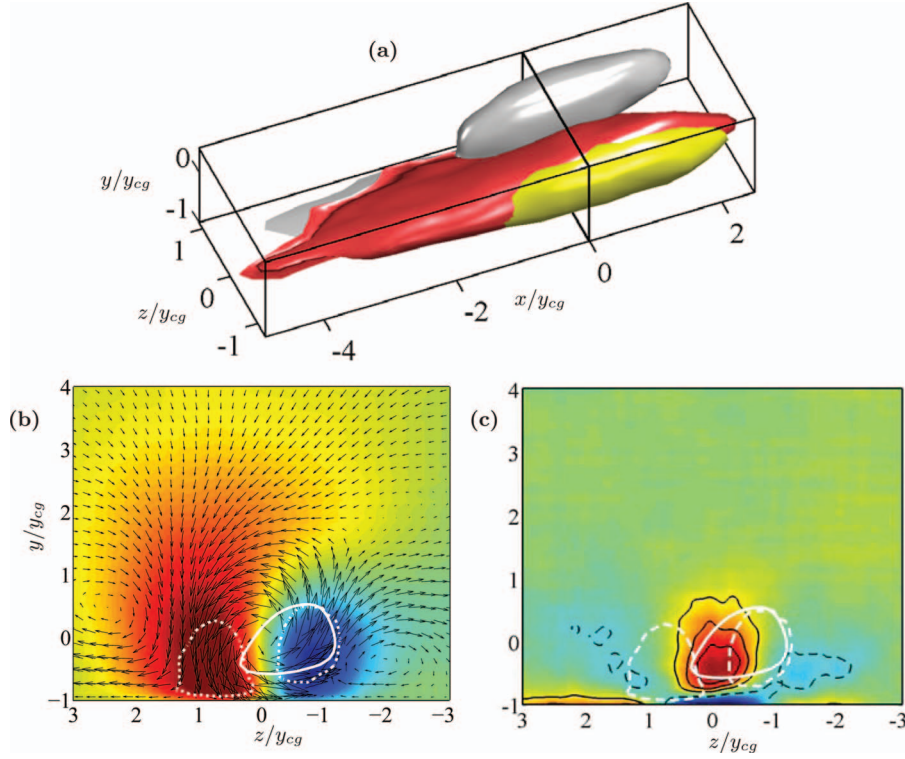
FIG. 9. (a) P.d.f.'s of the points belonging to the Q2 (yellow, front), Q4 (gray, back), and clusters (red, middle). The isosurfaces plotted are 0.75 times the maximum value of the p.d.f.'s for the Q's, and 0.85 for the cluster. Flow is from left to right, and coordinates are centered at the center of gravity of the sweep-ejection pair, and scaled with its distance to the wall. (b) Cross section of the conditional velocity field at $x = 0$ for the object in (a). The arrows are the cross-flow velocity (v, w), and the shaded map is the streamwise fluctuation velocity. The dark area to the right is $\tilde{u} < 0$, and the larger one to the left is $\tilde{u} > 0$. The white dotted lines are 0.75 times the maximum value of the p.d.f. of the points belonging to the Q's, and the white solid line is 0.85 times the maximum value of the p.d.f. of the points belonging to the cluster. Figures 9(a) and 9(b) are adapted from Ref. 103. (c) Cross section of the conditional streamwise vorticity field corresponding to the cross-flow velocities in (b). Color map and black contours are: ——, counter-clockwise vorticity, $\omega_x y_{cg}/u_\tau = 0.5(0.5)1.5$; – – –, clockwise, $\omega_x y_{cg}/u_\tau = -0.5$. The white contours are as in (b). Channel at $\delta^+ = 2003$,[33] including only structures taller than $y^+ = 100$.

Figure 9 is the best approximation that we have up to now of the mean physical structure of the attached Townsend[88] Reynolds-stress eddies discussed in Secs. II and III A.

IV. DYNAMICS

A. The buffer layer

Because of the strongest shear is concentrated near the wall, implying faster evolution times and higher energy production and dissipation, the dynamics of the buffer and logarithmic layers can be treated as relatively independent from the rest of the flow. We summarize first our current understanding of the dynamics of the buffer region, leaving the discussion of the logarithmic layer for a later section.

Soon after they were discovered,[7] it was proposed that the streaks and the vortices of the buffer layer are involved in a regeneration cycle in which the vortices are the results of an instability of the streaks,[117] and the streaks are created by the wall-normal advection of the streamwise velocity by the vortices.[118] Both processes have been documented and sharpened by numerical experiments. For example, Jiménez and Pinelli[12] showed that disturbing the streaks inhibits the formation of new vortices, while the existing ones decay at a rate consistent with the viscous damping of passive structures. This only works if it is done between $y^+ \approx 10$ and $y^+ \approx 60$, suggesting that the

primary regeneration cycle of the buffer layer works predominantly between those limits. There is a substantial body of numerical[71, 119, 120] and analytic[121, 122] work on the linear instability of sufficiently strong model streaks. The inflection points of their distorted velocity profiles are unstable to sinuous perturbations, and the eigenfunctions resemble the shape and location of the observed vortices. The model implied is a cycle in which streaks and vortices are created, grow, generate each other, and eventually decay. Additional references can be found in Ref. 12.

On the other hand, different explanations have been proposed, particularly for the instability of the streaks. It was shown by Schoppa and Hussain[71] that most streaks in the buffer layer are too weak to be unstable to the inflectional mechanism mentioned above, and, although the simplest explanation of that observation could be that unstable streaks are not observed because they have been destroyed by their instability, the question remains of precisely what is the energy source for the generation of the observed vortices, and of how do streaks retain their long streamwise coherence after breaking down to generate the vortices. Schoppa and Hussain[71] also remarked that the growth of the quasi-streamwise vortices in the buffer layer can be equally explained by the transient growth of structures in a shear[123, 124] as by inflectionally unstable eigenfunctions, and Butler and Farrell,[125] and later del Álamo and Jiménez[126] showed that many aspects of the velocity spectrum in channels can be reproduced by the temporal evolution of the most amplified perturbations of a suitably constrained linear model of the mean velocity profile. Similar results have been obtained for boundary layers,[127] and for the continuous random forcing of the mean flow.[128, 129] Those models do not require preexisting streaks, except perhaps as infinitesimal seed perturbations. Although the stability of a sheared streak may be difficult to tell apart from transient growth in a shear, the main difference between the two models is that the energy required to create the vortices is drawn from the streak in the first case, and directly from the much larger reservoir of the velocity difference across the mean shear in the second one. The difference is substantial. Even in the buffer layer, where the fluctuations are particularly strong, $u'^{2+} \approx 10$, the kinetic energy stored in the velocity differences across the mean profile is $U^{2+} \approx 100$. We will come back to this point when discussing the dynamics of the logarithmic layer.

An interesting observation is that, although the buffer layer is disorganized and chaotic,[14] the spatial chaos is not required to reproduce the turbulence statistics. Jiménez and Moin[130] performed simulations in which the near-wall region was substituted by an ordered "crystal" of surprisingly small identical "minimal" units, of approximate size 500×100 wall units in the streamwise and spanwise directions. Those are the dimensions of the small rectangle circled in Figure 3, which was identified in the discussion of that figure as the elemental structural unit of the buffer layer. Each minimal unit contains a single streamwise streak that crosses the box (and is therefore essentially infinite), and, on average, a pair of staggered quasi-streamwise vortices, in spite of which it reproduces fairly well the statistics of the full flow. Moreover, the dynamics of the layer below $y^+ \approx 60$ is autonomous, in the sense that the streaks and the vortices continue regenerating each other after the flow above them is artificially removed. That purely local cycle, with no forcing from the outer flow, also results in approximately correct statistics,[12] even in minimal computational boxes.[131]

Even further removed from the real flow, but also resulting in approximately correct statistics, are the three-dimensional nonlinear unstable traveling waves or weakly cyclical solutions of the Navier–Stokes equations, first obtained numerically for Couette flow at about the same time as the minimal unit just mentioned,[132] and later in many other situations.[25, 27, 133] Their dimensions are similar as those of the minimal units.

B. Bursting in the buffer layer

Notwithstanding the observation that the statistics of the flow are well approximated by steady or quasi-steady solutions, the flow is not steady. The time evolution of the near-wall structures is most easily studied in minimal boxes, because each box contains only a few structures whose evolution can be traced by analyzing the temporal behavior of the different quantities integrated over the whole minimal box. All those quantities "burst" quasi-periodically over time, with periods of the order of $T^+ = Tu_\tau^2/\nu \approx 400$.[58, 119, 130, 133] An example is given in Figure 10, which depicts the rising phase of a burst. As the streak becomes wavy and the streamwise vorticity fluctuations grow, Figure 10(a)
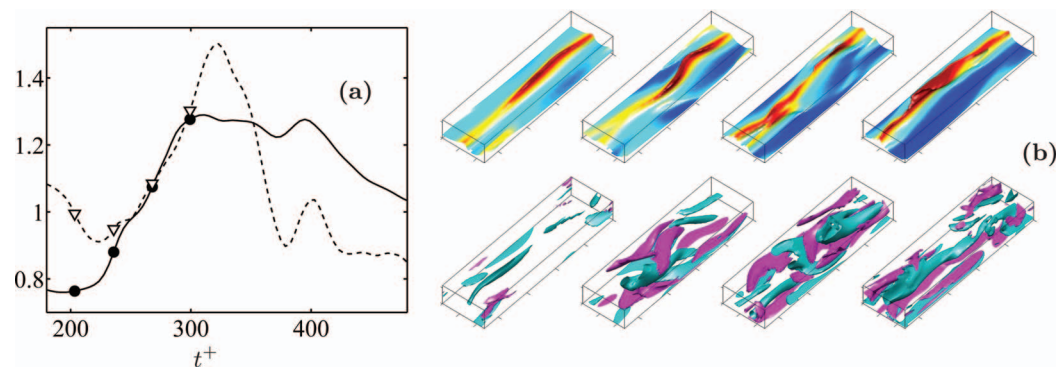
FIG. 10. Evolution of a minimal channel flow during a bursting event. $L_x^+ \times \delta^+ \times L_z^+ = 460 \times 180 \times 125$. (a) Evolution of the instantaneous: ——, box-averaged velocity gradient at the lower wall; – – –, box-averaged squared value of the streamwise-mean value of v, representing the instantaneous strength of the mean streamwise roller. Both quantities are normalized with their long-time mean. The symbols correspond to the snapshots on the right. (b) The top frames are isosurfaces $u^+ = 8$, colored by the distance to the wall, up to $y^+ = 30$ (dark to light). The bottom ones are $\omega_x^+ = 0.2$ (darker), and -0.2 (lighter). The flow is from bottom-left to top-right, and time marches towards the right. The top of the boxes is $y^+ = 60$, and the axes move with velocity $U_a^+ = 7.6$.

shows that the wall friction increases sharply, and so does the intensity of the wall-normal velocity. All quantities collapse rapidly after the burst.

Although the temporal bursting is clear in minimal boxes, whether full flows also burst needs to be proved. Bursting was originally introduced to describe the fluid eruptions observed near the wall in the early visualizations of turbulent boundary layers.[7, 8, 134] It was initially hypothesized that those bursts were due to the intermittent breakup of the near-wall streaks, but even the original authors later acknowledged that their visualizations could be consistent with permanent advecting objects,[135] and the term eventually became associated with the sweeps and ejections observed by stationary velocity probes. With the advent of numerical simulations, it became clear that the streaks are long-lived streamwise velocity structures, and that the ejections observed in single-point measurements were mostly due to the passing of groups of shorter quasi-streamwise vortices, intermittent in space but not necessarily in time.[136] The question of whether the observed temporally intermittent sublayer events were visualization artifacts or really existed in the near-wall layer was bypassed by this explanation.

To avoid confusion with the notation current at the time, the evidence of temporal intermittency in minimal boxes was originally described as "blooming,"[130] but the term did not catch. More recently, as new experiments and simulations have eroded the reliance of turbulence research on one-point measurements, the need for a special name for vortex passing has become less pressing, and "bursting" has been used again for temporally transient energetic events in shear turbulence.[24, 25, 133, 137, 138] It is in that sense that we use it here.

Of course, semantics says little about whether bursting in minimal boxes represents the behavior of full flows. Following the temporal evolution of individual structures in real flows has only recently been possible. Results are just beginning to appear,[10, 11] and some of them will be briefly summarized below. In the mean time, the best evidence for intermittent bursting in full flows is that the temporal variability of the statistics compiled in minimal boxes agrees well with the spatial variability of statistics compiled in randomly distributed sub-boxes of minimal size in full flows,[133] strongly suggesting that the bursting of the minimal boxes is indeed representative of the real flow.

The quasi-periodic bursting of the minimal boxes is most probably an artifact of the spatial periodicity, since the streaks in real flows move away from the location where they are created before they burst again. In a minimal periodic flow, the spatial periodicity brings the streak back into the simulation box but, in a real one, bursts would most likely be more or less independent from one another. All that probably remains is the average time elapsed from the moment in which the wall-normal velocity begins to strengthen and creates a new streak, until the streak erupts into a new burst.

If we define the burst by the behavior of either the streamwise vortices or of the wall-normal velocity, the bursting period given above is longer than the survival time of individual vortices, which decay viscously in $T^+ \approx 60$ when their production is artificially inhibited.[12] A similar time scale, $T^+ \approx 50$, can be extracted from the space-time spectra of the wall-normal velocity in flows not limited by their computational boxes.[95] The discrepancy between the vortex lifetimes and the longer bursting period in minimal boxes suggests that the regeneration cycle consists of relatively quiescent phases followed by shorter eruptions. Jiménez et al.[133] analyzed several minimal flows, and concluded that the bursting phase takes about one-third of the cycle, $T^+ \approx 100$, half of which is taken by the growth of the burst, and the other half by its decay.

Note that the bursting times just described are unrelated to the Eulerian bursting frequencies discussed in earlier papers in which sweeps and ejections were identified as they were advected past stationary probes.[139,140] Those results, most of which referred to events in the viscous near-wall layer, are essentially measures of the length and separation of the structures, and have been superseded by the spatial spectra discussed in Sec. III. Some of the early controversies about their Reynolds number scaling[141] can probably be traced to the multi-scale nature of the near-wall velocity spectrum, or even to instrumental limitations.[139]

In the inflectional-instability model, the growth time of the burst is presumably related to the internal velocity gradient of the streak, which is of the order of $u_\tau / \Delta z$. The implied growth time, $T^+ = O(\Delta z^+)$, is about a hundred wall units, compatible with the bursting times mentioned above. Unfortunately, this agreement cannot be used to discriminate between the inflectional-instability and transient-growth models for streak breakdown. In the transient-growth scenario, the characteristic deformation time of a structure of height $y^+ \approx 50$ would be of the order of its streamline wavelength, $\lambda_x^+ \approx 500$, divided by the velocity difference between the wall and the top of the perturbation, $U^+ \approx 10$. The result, $\lambda_x^+ / U^+ \approx 50$, is also of the right order of magnitude.

In summary, our best current understanding of the viscous and buffer layers is that the peak of the energy spectrum, at $\lambda_x^+ \times \lambda_z^+ \approx 500 \times 100$, is associated with structures that can be approximated by steady or weakly oscillating unstable traveling-wave solutions of the Navier-Stokes equations,[25,27,133] but which in reality undergo strong quasi-periodic bursting. As seen in Figure 10(b), and in related time histories in Refs. 12 and 130, the bursts create new vortices that in turn deform the streamwise velocity gradient into elemental streaks with lengths of the order of 500–1000 wall units. Those short segments subsequently aggregate into the longer objects observed in the sublayer,[27] although the details of the aggregation process are unclear. The regeneration cycle acts predominantly below $y^+ \lesssim 60$, and is able to run autonomously below that wall distance without input from the rest of the flow, even in minimal boxes. Although a similar cycle will be documented in Sec. IV C for the logarithmic layer, the results in the buffer region appear to be slightly different, presumably because of the influence of viscosity. For example, the low-velocity streaks are much longer than the high-speed ones below $y^+ \approx 50$, but the two velocity signs are roughly symmetric above that level.[27]

C. Bursting in the logarithmic layer

Minimal flow units are not restricted to the buffer layer, although the structures isolated by larger minimal boxes are not single streaks and vortices, but the complex structures described in Sec. III B. The key condition seems to be that the spanwise dimension of the simulation box is able to contain the wall-normal velocity spectrum. This is shown in Figure 11(a), which displays spectra of a large numerical box and of a smaller one, and shows that the latter develops correctly below the height at which it collides with the box dimensions. In fact, minimal boxes are only minimal over a slab of wall distances, centered around $y \approx L_z/3$, in which the wall-normal-velocity spectrum just fits into the box. The approximate limits of the minimal slab for the smaller box are marked in Figure 11(a). Below the bottom of the slab, turbulence does not feel the box, and develops with essentially correct statistics. Above the top, the spectrum is artificially constrained and the flow is disrupted.[138] In the minimal boxes discussed in Sec. IV B for the buffer layer, the minimal slab reaches from the wall to the top of the buffer layer, but bigger boxes have wall-detached minimal slabs.
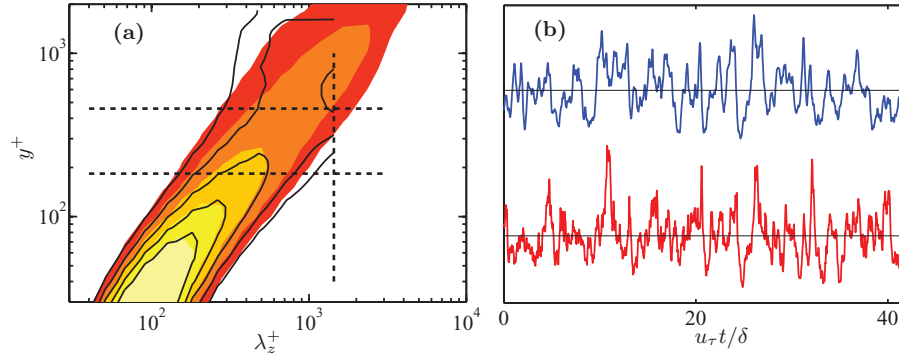
FIG. 11. (a) Premultiplied spectrum of the wall-normal velocity, as a function of the spanwise wavelength and of y. The shaded contours are a large channel at $\delta^+ = 2003$.[33] The line contours are a small box at $\delta^+ = 1850$, $L_x \times L_z = \pi\delta/2 \times \pi\delta/4$.[138] The vertical dashed line is the small-box L_z, and the two horizontal ones are the approximate limits of the minimal slab. (b) Temporal evolution of u^2 (top) and v^2 (bottom) integrated over the minimal slab of the small-channel simulation in (a). Each quantity is normalized with its long-time mean, and oscillates by about $\pm 20\%$.

Minimal boxes are conceptually important for several reasons. First, they show that the logarithmic layer is relatively independent of the flow above it, as was the case for the buffer layer, because the minimal slab develops normally even when the flow above it is constrained. Second, also as in the buffer layer, minimal boxes provide a convenient means to study in relative isolation the temporal evolution of the structures of the logarithmic layer, because the minimal slab contains a single large structure that can be studied by the evolution of slab-wide averages. Note that the spanwise dimensions involved, $L_z = 3y$ are an order of magnitude larger than the Corrsin scale, $L_c = 0.3y$, described in Sec. II A, so that minimal boxes are large enough to accommodate most of the anisotropic large scales responsible for the energy interactions with the mean shear.

It is interesting to note that the logarithmic layer is also essentially independent of the flow closer to the wall. The simplest evidence comes from the effect of rough walls, which destroy the dynamics of the buffer layer discussed above, and substitute it by the very different turbulence due to the wakes of the roughness elements. The properties of the logarithmic layer are only minimally modified by that substitution.[86, 88, 109, 142, 143] An even more direct test was performed by Mizuno and Jiménez,[144] who eliminated the buffer layer altogether, and substituted it by a synthetic boundary condition enforcing the velocity difference across the logarithmic layer, and mimicking the linear dependence of the length scale with the wall distance. Although the resulting flow was not ideal, it was close enough to a natural one to suggest that those are the only ingredients that the logarithmic layer draws from the wall. The strong suggestion from this apparent independence from the flow above and below it is that the logarithmic layer is basically a local shear flow, only weakly influenced by the neighborhood of the wall. The approximate agreement of the flow isotropy parameters in Figures 2(a) and 2(b) with other shear flows supports that conclusion.

The main result from minimal boxes in the logarithmic layer is that this part of the flow also bursts, and that the bursting process is very similar to that in the buffer layer.[138] This is shown in Figure 11(b), which displays the evolution of u^2 and v^2 integrated over the minimal slab, $y/\delta = 0.1$–0.25 ($y/L_z = 0.13$–0.3). Both quantities oscillate strongly, and the two histories are correlated enough to suggest that the oscillation is not random, but the effect of some common underlying process. The same is true for other variable pairs, involving in some cases a temporal delay. In the particular case of Figure 11(b), the correlation coefficient at zero-time delay is approximately 0.5, and reaches a maximum of about 0.6, with v^2 leading u^2 by about an eddy turnover time.[58] The evolution during a burst is shown in Figure 12, which should be compared to Figure 10. In both cases, a streak begins to bend while all the quantities in the box grow. Although not shown in the figure, the process is accompanied by the generation of copious small-scale vorticity. Eventually, as the streak breaks down, the burst collapses. The difference between Figures 10 and 12 is mainly one of scale. The latter is 15 times wider than the former, the streak is a turbulent object instead of a smooth one, and the time scale is about 10 times longer.
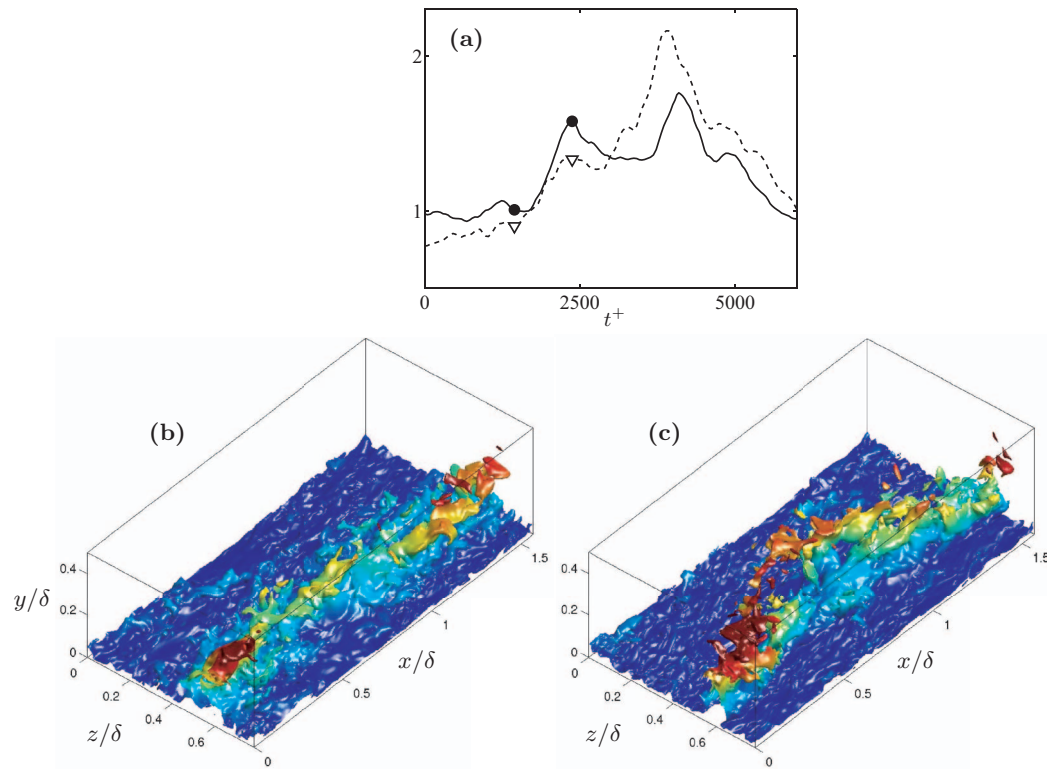
FIG. 12. Evolution of a logarithmic-layer minimal channel flow during a bursting event. (a) Evolution of: ——, v^2; – – –, enstrophy, both integrated over the slab $y/\delta = 0.1$–0.25, and normalized with their long-time mean. The symbols correspond to the snapshots below. (b) and (c) Isosurfaces $u^+ = 15$, colored by the distance to the wall, at the two moments marked by symbols in (a). Time increases from left to right. Box size is $L_x^+ \times L_z^+ = 2900 \times 1450$, and $\delta^+ = 1900$. Dark shades are close to the wall, and lighter ones are $y/\delta \approx 0.35$. Flow is from bottom left to top right. Adapted from Ref. 138.

The dynamics of bursting can be studied in more detail by examining the temporal correlation functions of slab-integrated quantities in minimal boxes.[58] Some examples of the autocorrelation function of v^2 are given in Figure 13(a), which can be used to define a bursting time scale from the width of the correlation at $C_{vv} = 0.5$. Other examples can be found in Ref. 58.

It turns out that the width of the autocorrelation is of the order of $S_m T \approx 8$, inversely proportional to the mean shear, S_m, at the center of the minimal slab.[58,138] For the logarithmic-layer structures in Figure 12 that is equivalent to $T^+ \approx 1000$, while for the buffer-layer ones in Figure 10, it is about $T^+ \approx 150$ if we take $y^+ = 40$. Because the shear in the logarithmic layer is inversely proportional to y, that rule implies that not only are all the dimensions of the structures in the logarithmic layer proportional to their height, but so is their bursting period.

The periods defined in this way are given in Figure 13(b) for three different small boxes at two Reynolds numbers, each of them measured for several bands of y. They collapse well, even if the mean shear differs between the different cases by factors of 2–4.

D. Full simulation boxes

Figure 13(b) also includes data from other sources. The two contours are p.d.f.'s of the lifetimes of individually tracked ejections in large computational boxes that do not artificially constrain the flow.[10] We have already mentioned that it has recently become feasible to compile databases of flow fields in computational boxes that are resolved both in space and in time, a possibility that had been previously prevented by the required storage. Lozano-Durán and Jiménez[10] used that opportunity to individually track in full-sized channels the Q's and vortex clusters described above. This was done in the range $\delta^+ = 1000$–4000, for enough eddy turnovers to compile statistics of several tens of
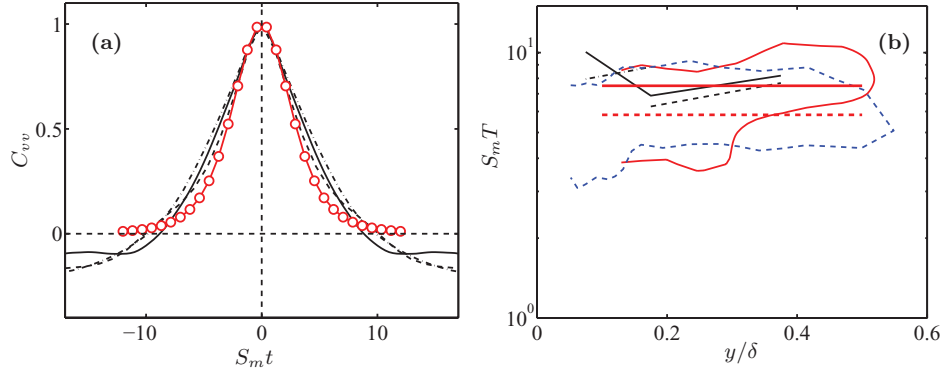
FIG. 13. (a) Temporal autocorrelation function of the slab-integrated v^2 in several minimal boxes. ——, $L_z = \pi/4, \delta^+ = 1850$; $- \cdot - \cdot -$, $L_z = \pi/8, \delta^+ = 1850$; $- - -$, $L_z = \pi/4, \delta^+ = 950$; $- \circ -$, linearized solution for an Orr burst, described in Sec. IV E. Adapted from Ref. 58. (b) Bursting periods in several flows, measured at $C_{vv} = 0.5$. Lines as function of y are as in (a). The horizontal solid line is from C_{vv} in a statistically stationary homogeneous shear flow.[56] The dashed horizontal line is from linearized homogeneous shear flow.[10] ——, $\delta^+ = 950$; $- - -$, $\delta^+ = 2000$. Each contour contains 80% of the cases. Times are normalized with the shear at the center of gravity of the perturbations at maximum intensity.

thousands of complete life histories. The full results will be reported elsewhere, but we summarize here the aspects related to bursting.

Individual vortex clusters and Q's are identified at each time step as in Ref. 103, and objects of the same kind that overlap sufficiently between consecutive time frames are identified as being part of the same life history. Histories interact continuously, with objects merging and splitting often. Most of these interactions involve the gain or loss of small fragments of the order of a few Kolmogorov scales, some of which are subsequently re-absorbed or lost again, but these interactions contribute relatively little to the growth or decay of the structures. Mergers and splits involving objects of comparable sizes can be considered events of a cascade, and account for a substantial part of the growth and decay of individual structures. The rest is due to the general continuous intensification or weakening of the eddy. During cascade events, it is usually possible to identify a largest object that can be defined as representing the main "branch," and branches constructed in this way can be tracked from birth to death.

Branches are not born at any particular distance from the wall, and most of them stay small, decay quickly, and move relatively little in height during their lives. However, some of them grow larger before decaying, and most of those which grow to be large enough, become attached to the wall at some point in their lives. Generally speaking, ejections move away from the wall, and so do clusters, but sweeps move towards it. The vertical migration speed of their center of gravity is approximately u_τ, in agreement with earlier results obtained in minimal boxes.[138] Note that, although the direction of these motions is not surprising, neither is it trivial. Sweeps and ejections are defined in terms of the velocities that they contain, not in terms of their movements as they migrate across the flow. For example, if a hairpin, carrying an ejection between its legs and two sweeps outside, were to rise from the wall, both the sweeps and the ejection would rise with it. The observation about the wall-normal migration of the Q's is therefore consistent with the single-roller model discussed at several points of this review.

Large structures spend about 2/3 of their lives attached to the wall, towards the end of their lives in sweeps, and towards the beginning in ejections. Clusters are intermediate between the two. As could be expected, the structures are sheared by the mean flow, which eventually destroys them. The advection velocity of each horizontal section of the structures is roughly the local mean velocity. Each branch can be given a characteristic height, such as the distance to the wall of its center of gravity at the moment in which its size is maximum, and it turns out that their lifetime is proportional to that height. As noted above, that can be interpreted as being inversely proportional to the local shear, which would agree with the interpretation that an important effect in determining their lifetimes is

their deformation by the mean velocity profile. The probability density functions of the lifetimes of ejections have been added to Figure 13(b). Considering that they refer to a different quantity than in the minimal boxes, and that they are obtained by a very different technique, they agree reasonably well.

Two more data sets are included in Figure 13. The first one is bursting in homogeneous shear turbulence. We have already mentioned that homogeneous turbulence bursts quasi-periodically when confined to finite computational boxes.[55,56] Although the bursting period depends somewhat on the geometrical aspect ratios of the box, there is a range of aspect ratios in which it only depends on the applied shear, and in which the integral parameters of the resulting turbulence agree well with those in channels.[56] The bursting period of that flow, computed by the temporal correlation method mentioned above, has been included as a horizontal line in Figure 13(b), and again agrees well with the other data.

E. Linearized models

The final data point added to Figure 13 is a linearized approximation to the evolution of the bursts. There is no argument that turbulence requires the nonlinearity of the Navier-Stokes equations. Neither multiscale cascades[4] nor the characteristic sensitivity to initial conditions[14] can exist in a statistically steady linear system. Nevertheless, there is also clear evidence that some aspects of shear turbulence are controlled by linear processes, especially in the energy-injection range. The best-known examples are the inflection-point linearized instabilities of the mean velocity profile,[6] which represent well many of the properties of the large-scale structures in fully nonlinear free-shear flows, especially forced ones.[145] The mean profiles of wall-bounded turbulence are known to be linearly stable,[146,147] but we have already mentioned that the larger scales in the flow interact strongly with the shear, at least near the wall. This has always been recognized, and there have been repeated attempts to relate the dynamics of those scales to linearized instabilities.[125–127,148] The general idea is that the ultimate energy source for turbulent fluctuations in a shear flow is the velocity difference across the mean profile, and that the main energy-production mechanism, the deformation of the profile by cross-shear velocities, is contained in the linearized equations. A key breakthrough took place when it was realized in the early 1990s that even linearly stable perturbations could grow substantially by extracting energy from the mean flow. For a review of such "transient-growth" mechanisms, see Ref. 124.

The agreement found in Figure 13(b) between the time scales of very different flows, with or without walls, and with uniform or inhomogeneous shear, suggests a common mechanism, and Jiménez[58] proposed that the common thread could be the transient mechanism proposed by Orr[149] for the amplification of the fluctuations of the vertical velocity in a shear. Briefly, Orr's mechanism is the response of continuity to the tilting of the structures by the mean flow. The vertical velocity is inhibited when the structures are closely stacked by tilting, and enhanced when they are deformed
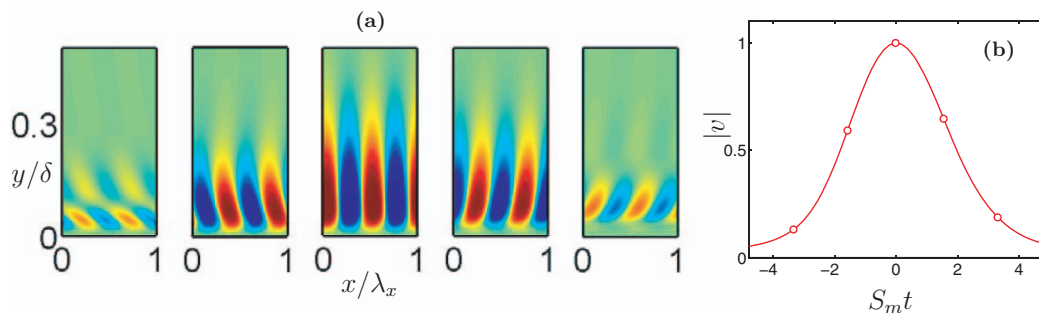

FIG. 14. (a) Evolution of nearly inviscid linearized v perturbations on the mean velocity profile of turbulent Poiseuille flow at $\delta^+ = 2000$.[58] The perturbation wavelength is $\lambda_x/\delta = 0.49$, and the five snapshots correspond to the symbols in (b). (b) L_2 norm of v as a function of time for the case in (a). The time is normalized with the shear at the center of gravity of the perturbation at $t = 0$.

into being normal to the flow direction. The mechanism is essentially inviscid, with characteristic times that scale with the shear, and results in a transient growth and decay closely resembling a model "burst." Although the cross-shear velocity of an Orr[149] burst eventually decays, it can create a streak of u that does not disappear when v does. Therefore, it can act as a mechanism to extract energy directly from the mean shear to the turbulent fluctuations, and has been discussed often in that connection. More references can be found in Ref. 58, and an example of its application to a turbulent channel profile is given in Figure 14. The temporal correlation C_{vv} of an Orr burst corresponding to the wavelength of the minimal boxes has been added to Figure 13(a), and the width of the resulting correlation has been added to Figure 13(b). Considering the simplifications involved, both of them agree surprisingly well with the real flow.

V. CONCLUSIONS

We have briefly reviewed the current status of our knowledge about wall-bounded turbulent flows, with special emphasis on the structural aspects, and on the layers near the wall where shear is dominant. These are the buffer and logarithmic layers, in which the Corrsin[57] shear parameter is $S^* \gg 1$. We have been especially interested in the logarithmic layer, about which less has been known until recently. In that layer, $S^* \approx 10$, and the shear interacts strongly with scales whose size is larger than about $y/3$. Smaller structures, and in particular the vorticity, decouple from the shear and become roughly isotropic away from the wall. The same is probably true for most structures above $y/\delta \approx 0.6$, where S^* approaches zero. Perhaps the most interesting conclusion from this part of the review is that, except possibly for the largest of the anisotropic scales, wall-bounded turbulence is mostly sheared turbulence, and is influenced relatively little by the presence of the wall. This agrees with evidence from numerical and laboratory experiments, such as roughness, that the statistics of the logarithmic layer are essentially independent of the flow above and below it.

We have reviewed the kinematics of the structures found in the shear-dominated layers. Near the wall, there is a single length scale, and structures are smooth. The important structures in this region are the well-known streamwise-velocity streaks and the quasi-streamwise vortices. The streaks contain most of the kinetic energy, and the vortices organize both the energy dissipation and the Reynolds stresses. These small-scale structures, of the order of a few hundreds wall units, are overlaid by much larger motions coming from the logarithmic and outer layers, but the scale difference is so large that most small scales live their whole life within a single large scale, which acts for them as a local boundary layer with its own friction velocity. Thus, during a typical lifetime of $t^+ \approx 400$, a sublayer streak moves with respect to the outer flow by about $\Delta x^+ = 3000$. Depending on the Reynolds number, this is typically much shorter than the large outer structures, which have sizes of the order of $\lambda_x = 10\delta$.

Above the buffer layer, the energy stays organized in streaks, although internally turbulent ones of much larger size than in the buffer layer, with spacings of the order of $2y$. On their part, the vortices lose the role of organizing the Reynolds stresses, which is taken over by turbulent eddies whose size is also $O(y)$. We have studied two kinds of eddies: vortex clusters and intense Reynolds stresses (ejections and sweeps). Both can be classified into a detached background and geometrically self-similar wall-attached families, whose lengths, widths, and lifetimes are proportional to their heights. The attached eddies are responsible for most of the momentum transfer, and associate themselves into groups formed by a sweep, an ejection to one side of it, and a vortex cluster loosely associated with the ejection. These groups sit in the interface between low- and high-velocity streaks, and are the best currently available model for the self-similar attached eddies hypothesized by Townsend.[88] The structure of these groups is compatible with a single streamwise large-scale roller, rather than with the twin legs of a hairpin. Their length is only $O(3y)$, but they tend to align themselves downstream from each other, resulting in an effectively much longer composite structure. The alignment mechanism is unknown.

The detached component appears to be common to other turbulent flows, is roughly isotropic, and contributes little to the net momentum transfer, because, although the individual eddies are as strong as the attached ones, and exist at all scales, their contributions cancel on average.

We have used a variety of techniques, including temporal correlations in minimal boxes and direct tracking of the structures in full-sized simulations, to show that an important characteristic of wall-bounded turbulence is temporally intermittent bursting at all distances from the wall. In particular, we have shown that the time scale of bursting in minimal boxes is a few shear times ($ST \approx 5 - 10$) when the shear is measured at the height of the bursting structure. We have shown that those times agree with the lifetimes of sweeps, ejections, and vortex clusters directly tracked in large numerical boxes for which the box size is not an issue. We have also shown that the self-similar attached structures are sheared by the mean velocity profile, with advection velocities that are approximately equal to the mean velocity at each wall distance.[150] Since this shearing distorts the structures in a few shear times, the strong suggestion is that it is responsible for limiting their lifetimes. This conclusion is reinforced by the observation that bursting in wall-bounded turbulence has a similar time scale to bursting in other shear flows, and in particular in uniformly sheared turbulence that cannot be influenced by a wall. The implied model is largely linear, with bursting controlled by the interaction of the eddies with the mean flow, rather than by nonlinear interactions with each other, and we have proposed that the underlying mechanism is the, possibly nonlinear, transient amplification by shear of the vertical velocity, as proposed by Orr.[149] The time scales involved are correct.[58]

A final observation regards the very large scales beyond the self-similar regime just discussed. The eddy dimensions in Figure 8(b) are consistent with the linear scaling of the length scales in the logarithmic layer, but the proportionality ceases to hold above $y = \delta$. That part of the p.d.f. represents very large objects that span both halves of the channel, and are thus very far from being linked to the logarithmic layer. Their true length is unknown, because results such as those in Figure 8(b) are limited by the length of the simulation box. The same is true of most experiments. Note also that, because the advection velocity of very large scales is approximately constant across the channel, instead of changing with the distance to the wall,[150] the lifetime of these structures need not be limited by the shearing effect discussed above. Examination of their temporal behavior in simulations shows that they are extremely persistent.

Experimental temporal spectra at very high Reynolds numbers suggests that the longest structures in Figure 8(b), $L_x \approx 20\delta$, may be close to their maximum real length,[79] but, from the point of view of the other structures in the flow, they are infinitely long in the same way that the sublayer streaks are much longer than their associated vortices. They have been variously described as global modes[31,102] or very large scales,[22,23] and their possible origin has been the subject of a fair amount of speculation. In many of those discussions, they are treated as structures of the streamwise velocity with little Reynolds stress,[79] but the eddies in Figure 8(b) are Reynolds-stress structures, and are therefore active in momentum transfer.[151] That issue is beyond the scope of this paper, but some recent work suggests that there may be a quasi-two-dimensional mechanism for the maintenance of turbulence whose result would be essentially infinite rolls.[129,152] Paradoxically, the older simulations in Ref. 153 of channels with very short streamwise dimensions may also point to a different, but also quasi-two-dimensional, turbulence dynamics in the cross plane.

[1] A. A. Townsend, "Equilibrium layers and wall turbulence," J. Fluid Mech. **11**, 97–120 (1961).
[2] L. F. Richardson, "The supply of energy from and to atmospheric eddies," Proc. R. Soc. London, Ser. A **97**, 354–373 (1920).
[3] O. Reynolds, "On the dynamical theory of incompressible viscous fluids and the determination of the criterion," Philos. Trans. R. Soc. London **186**, 123–164 (1895).

[4] A. N. Kolmogorov, "The local structure of turbulence in incompressible viscous fluids for very large Reynolds numbers," Dokl. Akad. Nauk SSSR **30**, 301–305 (1941), reprinted in Proc. R. Soc. London, Ser. A **434**, 9–13 (1991).

[5] A. M. Obukhov, "On the distribution of energy in the spectrum of turbulent flow," Dokl. Akad. Nauk SSSR **32**, 22–24 (1941).

[6] G. L. Brown and A. Roshko, "On the density effects and large structure in turbulent mixing layers," J. Fluid Mech. **64**, 775–816 (1974).

[7] S. J. Kline, W. C. Reynolds, F. A. Schraub, and P. W. Runstadler, "Structure of turbulent boundary layers," J. Fluid Mech. **30**, 741–773 (1967).

[8] E. R. Corino and R. S. Brodkey, "A visual investigation of the wall region in turbulent flow," J. Fluid Mech. **37**, 1–30 (1969).

[9] E. Perlman, R. Burns, Y. Li, and C. Meneveau, "Data exploration of turbulence simulations using a database cluster," in *Proceedings of the ACM/IEEE Supercomputing Conference 07* (ACM, New York, 2007), pp. 23.1–23.11.

[10] A. Lozano-Durán and J. Jiménez, "Time-resolved evolution of the wall-bounded vorticity cascade," J. Phys.: Conf. Ser. **318**, 062016 (2011).

[11] J. A. LeHew, M. Guala, and B. J. McKeon, "Time-resolved measurements of coherent structures in the turbulent boundary layer," Exp. Fluids **54**, 1508 (2013).

[12] J. Jiménez and A. Pinelli, "The autonomous cycle of near wall turbulence," J. Fluid Mech. **389**, 335–359 (1999).

[13] H. Tennekes and J. L. Lumley, *A First Course in Turbulence* (MIT Press, 1972).

[14] L. Keefe, P. Moin, and J. Kim, "The dimension of attractors underlying periodic turbulent poiseuille flow," J. Fluid Mech. **242**, 1–29 (1992).

[15] R. Temam, *Navier–Stokes Equations and Nonlinear Functional Analysis*, 2nd ed. (SIAM, 1995).

[16] R. H. Kraichnan, "Inertial range transfer in two- and three-dimensional turbulence," J. Fluid Mech. **47**, 525–535 (1971).

[17] M. Lesieur, *Turbulence in Fluids*, 4th ed. (Springer, 2008), Chap. 10.

[18] G. Kawahara, "Laminarization of minimal plane Couette flow: Going beyond the basin of attraction of turbulence," Phys. Fluids **17**, 041702 (2005).

[19] G. H. L. Hagen, "Über den Bewegung des Wassers in engen cylindrischen Röhren," Pogg. Ann. Phys. Chem. **46**, 423–442 (1839).

[20] H. Darcy, "Recherches expérimentales rélatives au mouvement de l'eau dans les tuyeaux," Mém. Savants Etrang. Acad. Sci. Paris **17**, 1–268 (1854).

[21] International Energy Agency, *Key World Energy Statistics* (IEA, Paris, 2012), available from http://www.iea.org/publications/freepublications/publication/kwes.pdf.

[22] R. J. Adrian, "Hairpin vortex organization in wall turbulence," Phys. Fluids **19**, 041301 (2007).

[23] A. J. Smits, B. J. McKeon, and I. Marusic, "High-Reynolds number wall turbulence," Annu. Rev. Fluid Mech. **43**, 353–375 (2011).

[24] J. Jiménez, "Cascades in wall-bounded turbulence," Annu. Rev. Fluid Mech. **44**, 27–45 (2012).

[25] G. Kawahara, M. Uhlmann, and L. van Veen, "The significance of simple invariant solutions in turbulent flows," Annu. Rev. Fluid Mech. **44**, 203–225 (2012).

[26] I. Marusic, and R. J. Adrian, "The eddies and scales of wall turbulence," in *Ten Chapters in Turbulence*, edited by P. A. Davidson, Y. Kaneda, and K. R. Sreenivasan (Cambridge University Press, 2013), pp. 176–220.

[27] J. Jiménez and G. Kawahara, "Dynamics of wall-bounded turbulence," in *Ten Chapters in Turbulence*, edited by P. A. Davidson, Y. Kaneda, and K. R. Sreenivasan (Cambridge University Press, 2013), pp. 221–268.

[28] J. Kim, P. Moin, and R. D. Moser, "Turbulence statistics in fully developed channel flow at low Reynolds number," J. Fluid Mech. **177**, 133–166 (1987).

[29] E. D. Siggia, "Numerical study of small scale intermittency in three-dimensional turbulence," J. Fluid Mech. **107**, 375–406 (1981).

[30] R. S. Rogallo, "Numerical experiments in homogeneous turbulence," Technical Memo 81315 (NASA, 1981).

[31] J. C. del Álamo, J. Jiménez, P. Zandonade, and R. D. Moser, "Scaling of the energy spectra of turbulent channels," J. Fluid Mech. **500**, 135–144 (2004).

[32] H. Abe, H. Kawamura, and Y. Matsuo, "Surface heat-flux fluctuations in a turbulent channel flow up to $Re_\tau = 1020$ with $Pr = 0.025$ and 0.71," Int. J. Heat Fluid Flow **25**, 404–419 (2004).

[33] S. Hoyas and J. Jiménez, "Scaling of the velocity fluctuations in turbulent channels up to $Re_\tau = 2003$," Phys. Fluids **18**, 011702 (2006).

[34] J.-H. Lee and H. J. Sung, "Direct numerical simulation of the turbulent boundary layer over a rod-roughened wall," J. Fluid Mech. **584**, 125–146 (2007).

[35] J.-H. Lee and H. J. Sung, "Very-large-scale motions in a turbulent boundary layer," J. Fluid Mech. **673**, 80–120 (2011).

[36] J. Jiménez, S. Hoyas, M. P. Simens, and Y. Mizuno, "Turbulent boundary layers and channels at moderate Reynolds numbers," J. Fluid Mech. **657**, 335–360 (2010).

[37] X. Wu and P. Moin, "Transitional and turbulent boundary layer with heat transfer," Phys. Fluids **22**, 085105 (2010).

[38] P. Schlatter, R. Örlü, Q. Li, J. H. M. Fransson, A. V. Johansson, P. H. Alfredsson, and D. S. Henningson, "Turbulent boundary layers up to $Re_\theta = 2500$ through simulation and experiments," Phys. Fluids **21**, 051702 (2009).

[39] P. Schlatter and R. Örlü, "Assessment of direct numerical simulation data of turbulent boundary layers," J. Fluid Mech. **659**, 116–126 (2010).

[40] J. A. Sillero, G. Borrell, A. G. Gungor, J. Jiménez, R. Moser, and T. A. Oliver, "Direct simulation of the zero-pressure-gradient boundary layer up to $Re_\theta = 6000$," Bull. Am. Phys. Soc. **55**(16), EB.4 (2010).

[41] X. Wu and P. Moin, "A direct numerical simulation study on the mean velocity characteristics in turbulent pipe flow," J. Fluid Mech. **608**, 81–112 (2008).

[42] B. J. Boersma, "Direct numerical simulation of turbulent pipe flow up to a Reynolds number of 61,000," J. Phys.: Conf. Ser. **318**, 042045 (2011).

[43] J.-H. Lee and H. J. Sung, "Comparison of very-large-scale motions of turbulent pipe and boundary layer simulations," Phys. Fluids **25**, 045103 (2013).

[44] A. Lozano-Durán, private communication (2012).

[45] S. Pirozzoli and M. Bernardini, "Probing high-Reynolds-number effects in numerical boundary layers," Phys. Fluids **25**, 021704 (2013).

[46] J. Jiménez, "Computing high-Reynolds number flows: will simulations ever substitute experiments?" J. Turbul. **4**, N22 (2003).

[47] S. G. Saddoughi and S. V. Veeravali, "Local isotropy in turbulent boundary layers at high Reynolds numbers," J. Fluid Mech. **268**, 333–372 (1994).

[48] J. M. Österlund, A. V. Johansson, H. M. Nagib, and M. Hites, "A note on the overlap region in turbulent boundary layers," Phys. Fluids **12**, 1–4 (2000).

[49] C. B. Millikan, "A critical discussion of turbulent flows in channels and circular tubes," in *Proceedings of the 5th International Conference on Applied Mechanics* (Wiley, 1938), pp. 386–392.

[50] M. van Dyke, *Perturbation Methods in Fluid Mechanics*, 2nd ed. (The Parabolic Press, Stanford, 1975).

[51] N. Afzal and K. Yajnik, "Analysis of turbulent pipe and channel flows at moderately large Reynolds number," J. Fluid Mech. **61**, 23 (1973).

[52] J. Jiménez and R. D. Moser, "What are we learning from simulating wall turbulence?" Philos. Trans. R. Soc. A **365**, 715 (2007).

[53] M. V. Zagarola and A. J. Smits, "Scaling of the mean velocity profile for turbulent pipe shear flows," Phys. Rev. Lett. **78**, 239–242 (1997).

[54] G. K. Batchelor, *The Theory of Homogeneous Turbulence* (Cambridge University Press, 1953).

[55] A. Pumir, "Turbulence in homogeneous shear flows," Phys. Fluids **8**, 3112–3127 (1996).

[56] S. Dong, A. Sekimoto, and J. Jiménez, "The effect of aspect ratio on statistically-stationary homogeneous shear flow," Bull. Am. Phys. Soc. **57**(17), D21.7 (2012).

[57] S. Corrsin, "Local isotropy in turbulent shear flow," Research Memo 58B11 (NACA, 1958).

[58] J. Jiménez, "How linear is wall-bounded turbulence?" Phys. Fluids **25**, 110814 (2013).

[59] M. J. Lee, J. Kim, and P. Moin, "Structure of turbulence at high shear rates," J. Fluid Mech. **216**, 561–583 (1990).

[60] J. L. Lumley, "Computational models of turbulent flows," Adv. Appl. Mech. **18**, 123–176 (1979).

[61] S. B. Pope, *Turbulent Flows* (Cambridge University Press, 2000).

[62] M. M. Rogers and P. Moin, "The structure of the vorticity field in homogeneous turbulent flows," J. Fluid Mech. **176**, 33–66 (1987).

[63] S. Kida and M. Tanaka, "Dynamics of vortical structures in a homogeneous shear flow," J. Fluid Mech. **274**, 43–68 (1994).

[64] J. L. Lumley, "Similarity and the turbulent energy spectrum," Phys. Fluids **10**, 855–858 (1967).

[65] T. Ishihara, K. Yoshida, and Y. Kaneda, "Anisotropic velocity correlation spectrum at small scales in a homogeneous turbulent shear layer," Phys. Rev. Lett. **88**, 154501 (2002).

[66] C. R. Smith and S. P. Metzler, "The characteristics of low speed streaks in the near wall region of a turbulent boundary layer," J. Fluid Mech. **129**, 27–54 (1983).

[67] J. C. Klewicki, M. M. Metzger, E. Kelner, and E. M. Thurlow, "Viscous sublayer flow visualizations at $R_\theta \approx 1,500,000$," Phys. Fluids **7**, 857–863 (1995).

[68] G. J. Kunkel and I. Marusic, "Study of the near-wall-turbulent region of the high-Reynolds-number boundary layer using atmospheric data," J. Fluid Mech. **548**, 375–402 (2006).

[69] P. Moin and R. D. Moser, "Characteristic-eddy decomposition of turbulence in a channel," J. Fluid Mech. **200**, 471–509 (1989).

[70] J. Jiménez, J. C. del Álamo, and O. Flores, "The large-scale dynamics of near-wall turbulence," J. Fluid Mech. **505**, 179–199 (2004).

[71] W. Schoppa and F. Hussain, "Coherent structure generation in near-wall turbulence," J. Fluid Mech. **453**, 57–108 (2002).

[72] N. Hutchins and I. Marusic, "Evidence of very long meandering features in the logarithmic region of turbulent boundary layers," J. Fluid Mech. **579**, 1–28 (2007).

[73] D. B. de Graaff and J. K. Eaton, "Reynolds number scaling of the flat-plate turbulent boundary layer," J. Fluid Mech. **422**, 319–346 (2000).

[74] M. Metzger and J. Klewicki, "A comparative study of near-wall turbulence in high and low Reynolds number boundary layers," Phys. Fluids **13**, 692–701 (2001).

[75] M. Metzger, J. Klewicki, K. Bradshaw, and R. Sadr, "Scaling of near-wall axial turbulent stress in the zero pressure gradient boundary layer," Phys. Fluids **13**, 1819–1821 (2001).

[76] I. Marusic and G. J. Kunkel, "Streamwise turbulence intensity formulation for flat-plate boundary layers," Phys. Fluids **15**, 2461–2464 (2003).

[77] H. C. H. Ng, J. P. Monty, N. Hutchins, M. S. Chong, and I. Marusic, "Comparison of turbulent channel and pipe flows with varying Reynolds number," Exp. Fluids **51**, 1261–1281 (2011).

[78] J. A. Sillero, J. Jiménez, and R. D. Moser, "One-point statistics for turbulent wall-bounded flows at Reynolds numbers up to $\delta^+ \approx 2000$," Phys. Fluids **25**, 105102 (2013).

[79] J. Jiménez and S. Hoyas, "Turbulent fluctuations above the buffer layer of wall-bounded flows," J. Fluid Mech. **611**, 215–236 (2008).

[80] J. P. Monty, N. Hutchins, H. C. H. Ng, I. Marusic, and M. S. Chong, "A comparison of turbulent pipe, channel and boundary layer flows," J. Fluid Mech. **632**, 431–442 (2009).

[81] J. A. Sillero, J. Jiménez, and R. Moser, "Two-point correlations for zero-pressure-gradient turbulent boundary layers and channels at $Re_\tau = 1000 - 2000$," Bull. Am. Phys. Soc. **57**(17), D20.7 (2012).

[82] R. Mathis, N. Hutchins, and I. Marusic, "Large-scale amplitude modulation of the small-scale structures in turbulent boundary layers," J. Fluid Mech. **628**, 311–337 (2009).

[83] J. W. Deardorff, "A numerical study of three-dimensional turbulent channel flow at large Reynolds numbers," J. Fluid Mech. **41**, 453–480 (1970).

[84] U. Schumann, "Subgrid-scale model for finite difference simulation of turbulent flows in plane channels and annuli," J. Comput. Phys. **18**, 376–404 (1975).

[85] U. Piomelli, "Wall-layer models for large-eddy simulations," Prog. Aerosp. Sci. **44**, 437–446 (2008).

[86] A. E. Perry and C. J. Abell, "Asymptotic similarity of turbulence structures in smooth- and rough-walled pipes," J. Fluid Mech. **79**, 785–799 (1977).

[87] A. E. Perry, S. M. Henbest, and M. S. Chong, "A theoretical and experimental study of wall turbulence," J. Fluid Mech. **165**, 163–199 (1986).

[88] A. A. Townsend, *The Structure of Turbulent Shear Flow*, 2nd ed. (Cambridge University Press, 1976), Chap. 3.12.

[89] P. Bradshaw, "Inactive motions and pressure fluctuations in turbulent boundary layers," J. Fluid Mech. **30**, 241–258 (1967).

[90] F. Tuerke and J. Jiménez, "Simulations of turbulent channels with prescribed velocity profiles," J. Fluid Mech. **723**, 587–603 (2013).

[91] A. E. Perry and M. S. Chong, "On the mechanism of wall turbulence," J. Fluid Mech. **119**, 173–217 (1982).

[92] M. Hultmark, M. Vallikivi, S. C. C. Bailey, and A. J. Smits, "Turbulent pipe flow at extreme Reynolds numbers," Phys. Rev. Lett. **108**, 094501 (2012).

[93] I. Marusic, J. P. Monty, M. Hultmark, and A. J. Smits, "On the logarithmic region in wall turbulence," J. Fluid Mech. **716**, R3 (2013).

[94] J. A. Sillero, J. Jiménez, R. D. Moser, and N. P. Malaya, "Direct simulation of a zero-pressure-gradient turbulent boundary layer up to $Re_\theta = 6650$," J. Phys.: Conf. Ser. **318**, 022023 (2011).

[95] J. C. del Álamo, J. Jiménez, P. Zandonade, and R. D. Moser, "Self-similar vortex clusters in the logarithmic region," J. Fluid Mech. **561**, 329–358 (2006).

[96] M. Farge, "Wavelet transforms and their applications to turbulence," Annu. Rev. Fluid Mech. **24**, 395–457 (1992).

[97] M. Farge, G. G. Pellegrino, and K. Schneider, "Coherent vortex extraction in 3D turbulent flows using orthogonal wavelets," Phys. Rev. Lett. **87**, 054501 (2001).

[98] C. D. Winant and F. K. Browand, "Vortex pairing: The mechanism of turbulent mixing-layer growth at moderate Reynolds number," J. Fluid Mech. **63**, 237–255 (1974).

[99] Z. She, E. Jackson, and S. A. Orszag, "Intermittent vortex structures in homogeneous isotropic turbulence," Nature (London) **344**, 226–228 (1990).

[100] A. Vincent and M. Meneguzzi, "The spatial structure and statistical properties of homogeneous turbulence," J. Fluid Mech. **225**, 1–20 (1991).

[101] J. Jiménez, A. A. Wray, P. G. Saffman, and R. S. Rogallo, "The structure of intense vorticity in isotropic turbulence," J. Fluid Mech. **255**, 65–90 (1993).

[102] J. C. del Álamo and J. Jiménez, "Spectra of very large anisotropic scales in turbulent channels," Phys. Fluids **15**, L41–L44 (2003).

[103] A. Lozano-Durán, O. Flores, and J. Jiménez, "The three-dimensional structure of momentum transfer in turbulent channels," J. Fluid Mech. **694**, 100–130 (2012).

[104] J. Jiménez and A. A. Wray, "On the characteristic of vortex filaments in isotropic turbulence," J. Fluid Mech. **373**, 255–285 (1998).

[105] J. Jiménez, F. Moisy, P. Tabeling, and H. Willaime, "Scaling and structure in isotropic turbulence," in *Intermittency in Turbulent Flows*, edited by J. C. Vassilicos (Cambridge University Press, 2000), pp. 193–212.

[106] M. Tanahashi, S. Iwase, and T. Miyauchi, "Appearance and alignment of strain rate of coherent fine scale eddies in turbulent mixing layer," J. Turbul. **2**, 1–17 (2001).

[107] M. Tanahashi, S.-J. Kang, T. Miyamoto, S. Shiokawa, and T. Miyauchi, "Scaling law of fine scale eddies in turbulent channel flow at to $Re_\tau = 800$," Int. J. Heat Fluid Flow **25**, 331–340 (2004).

[108] F. Moisy and J. Jiménez, "Geometry and clustering of intense structures in isotropic turbulence," J. Fluid Mech. **513**, 111–133 (2004).

[109] O. Flores and J. Jiménez, "Effect of wall-boundary disturbances on turbulent channel flows," J. Fluid Mech. **566**, 357–376 (2006).

[110] J. M. Wallace, H. Eckelman, and R. S. Brodkey, "The wall region in turbulent shear flow," J Fluid Mech. **54**, 39–48 (1972).

[111] W. W. Willmarth and S. S. Lu, "Structure of the Reynolds stress near the wall," J. Fluid Mech. **55**, 65–92 (1972).

[112] S. S. Lu and W. W. Willmarth, "Measurements of the structure of the Reynolds stress in a turbulent boundary layer," J. Fluid Mech. **60**, 481–511 (1973).

[113] R. S. Brodkey, J. M. Wallace, and H. Eckelman, "Some properties of truncated turbulence signals in bounded shear flows," J. Fluid Mech. **63**, 209–224 (1974).

[114] D. G. Bogard and W. G. Tiederman, "Burst detection with single-point velocity measurements," J. Fluid Mech. **162**, 389–413 (1986).

[115] R. F. Blackwelder and R. E. Kaplan, "On the wall structure of the turbulent boundary layer," J. Fluid Mech. **76**, 89–112 (1976).

[116] J. Kim, "Turbulence structures associated with the bursting event," Phys. Fluids **28**, 52–58 (1985).

[117] J. D. Swearingen and R. F. Blackwelder, "The growth and breakdown of streamwise vortices in the presence of a wall," J. Fluid Mech. **182**, 255–290 (1987).

[118] H. P. Bakewell and J. L. Lumley, "Viscous sublayer and adjacent wall region in turbulent pipe flow," Phys. Fluids **10**, 1880–1889 (1967).

[119] J. M. Hamilton, J. Kim, and F. Waleffe, "Regeneration mechanisms of near-wall turbulence structures," J. Fluid Mech. **287**, 317–248 (1995).

[120] F. Waleffe, "On a self-sustaining process in shear flows," Phys. Fluids **9**, 883–900 (1997).

[121] S. C. Reddy, P. J. Schmid, J. S. Baggett, and D. S. Henningson, "On stability of streamwise streaks and transition thresholds in plane channel flows," J. Fluid Mech. **365**, 269–303 (1998).

[122] G. Kawahara, J. Jiménez, M. Uhlmann, and A. Pinelli, "Linear instability of a corrugated vortex sheet – a model for streak instability," J. Fluid Mech. **483**, 315–342 (2003).

[123] P. J. Schmid and D. S. Henningson, *Stability and Transition in Shear Flows* (Springer, 2001), pp. 55–58.

[124] P. J. Schmid, "Nonmodal stability theory," Annu. Rev. Fluid Mech. **39**, 129–162 (2007).

[125] K. M. Butler and B. F. Farrell, "Optimal perturbations and streak spacing in wall-bounded shear flow," Phys. Fluids A **5**, 774–777 (1993).

[126] J. C. del Álamo and J. Jiménez, "Linear energy amplification in turbulent channels," J. Fluid Mech. **559**, 205–213 (2006).

[127] C. Cossu, G. Pujals, and S. Depardon, "Optimal transient growth and very large-scale structures in turbulent boundary layers," J. Fluid Mech. **619**, 79–94 (2009).

[128] B. F. Farrell and P. J. Ioannou, "Stochastic forcing of the linearized Navier–Stokes equations," Phys. Fluids A **5**, 2600–2609 (1993).

[129] D. F. Gayme, B. J. McKeon, B. Bamieh, A. Papachristodoulou, and J. C. Doyle, "Amplification and nonlinear mechanisms in plane Couette flow," Phys. Fluids **23**, 065108 (2011).

[130] J. Jiménez and P. Moin, "The minimal flow unit in near-wall turbulence," J. Fluid Mech. **225**, 213–240 (1991).

[131] J. Jiménez and M. P. Simens, "Low-dimensional dynamics in a turbulent wall flow," J. Fluid Mech. **435**, 81–91 (2001).

[132] M. Nagata, "Three-dimensional finite-amplitude solutions in plane Couette flow: Bifurcation from infinity," J. Fluid Mech. **217**, 519–527 (1990).

[133] J. Jiménez, G. Kawahara, M. P. Simens, M. Nagata, and M. Shiba, "Characterization of near-wall turbulence in terms of equilibrium and 'bursting' solutions," Phys. Fluids **17**, 015105 (2005).

[134] H. T. Kim, S. J. Kline, and W. C. Reynolds, "The production of turbulence near a smooth wall in a turbulent boundary layer," J. Fluid Mech. **50**, 133–160 (1971).

[135] G. R. Offen and S. J. Kline, "A proposed model for the bursting process in turbulent boundary layers," J. Fluid Mech. **70**, 209–228 (1975).

[136] S. K. Robinson, "Coherent motions in the turbulent boundary layer," Annu. Rev. Fluid Mech. **23**, 601–639 (1991).

[137] G. Kawahara and S. Kida, "Periodic motion embedded in plane Couette turbulence: Regeneration cycle and burst," J. Fluid Mech. **449**, 291–300 (2001).

[138] O. Flores and J. Jiménez, "Hierarchy of minimal flow units in the logarithmic layer," Phys. Fluids **22**, 071704 (2010).

[139] R. F. Blackwelder and J. H. Haritonidis, "Scaling of the bursting frequency in turbulent boundary layers," J. Fluid Mech. **132**, 87–103 (1983).

[140] T. S. Luchik and W. G. Tiederman, "Timescale and structure of ejections and bursts in turbulent channel flows," J. Fluid Mech. **174**, 529–552 (1987).

[141] K. N. Rao, R. Narasimha, and M. A. B. Narayanan, "The bursting phenomenon in a turbulent boundary layer," J. Fluid Mech. **48**, 339–352 (1971).

[142] J. Jiménez, "Turbulent flows over rough walls," Annu. Rev. Fluid Mech. **36**, 173–196 (2004).

[143] M. P. Schultz and K. A. Flack, "The rough-wall turbulent boundary layer from the hydraulically smooth to the fully rough regime," J. Fluid Mech. **580**, 381–405 (2007).

[144] Y. Mizuno and J. Jiménez, "Wall turbulence without walls," J. Fluid Mech. **723**, 429–455 (2013).

[145] M. Gaster, E. Kit, and I. Wygnanski, "Large-scale structures in a forced turbulent mixing layer," J. Fluid Mech. **150**, 23–39 (1985).

[146] W. C. Reynolds and W. G. Tiederman, "Stability of turbulent channel flow, with application to Malkus' theory," J. Fluid Mech. **27**, 253–272 (1967).

[147] A. K. M. F. Hussain and W. C. Reynolds, "The mechanics of an organized wave in turbulent shear flow," J. Fluid Mech. **41**, 241–258 (1970).

[148] W. V. R. Malkus, "Outline of a theory of turbulent shear flow," J. Fluid Mech. **1**, 521–539 (1956).

[149] W. M. Orr, "The stability or instability of the steady motions of a perfect liquid, and of a viscous liquid. Part I: A perfect liquid," Proc. R. Ir. Acad. A **27**, 9–68 (1907).

[150] J. C. del Álamo and J. Jiménez, "Estimation of turbulent convection velocities and corrections to Taylor's approximation," J. Fluid Mech. **640**, 5–26 (2009).

[151] M. Guala, S. E. Hommema, and R. J. Adrian, "Large-scale and very-large-scale motions in turbulent pipe flow," J. Fluid Mech. **554**, 521–542 (2006).

[152] B. F. Farrell and P. J. Ioannou, "Dynamics of streamwise rolls and streaks in turbulent wall-bounded shear flow," J. Fluid Mech. **708**, 149–196 (2012).

[153] S. Toh and T. Itano, "Interaction between a large-scale structure and near-wall structures in channel flow," J. Fluid Mech. **524**, 249–262 (2005).